

**ULTRA-STRUCTURAL ANATOMY AND 3D RECONSTRUCTION
OF PLANT TISSUES AND ORGANELLES USING TRANSMISSION
ELECTRON MICROSCOPY AND FOCUSED ION BEAM
SCANNING ELECTRON MICROSCOPY**

By:

Bhawana

A Dissertation Submitted in Fulfillment
of the Requirements for the Doctoral Degree in
Molecular Biosciences

Middle Tennessee State University
December, 2014

Dissertation Committee:

Dr. Aubrey Bruce Cahoon, Chair

Dr. Anthony L. Farone

Dr. Jeffrey D. Leblond

Dr. Matthew Elrod-Erickson

Dr. Rebecca Seipelt-Thiemann

I dedicate this research to my sweet and loving,

Father and Mother,

who made me believe in myself and whose love, encouragement, guidance and praise
make me able to achieve such success and honor.

I love you, Ma and Papa, now and forever.

ACKNOWLEDGMENTS

I would like to thank my husband Harsh and both of our families for their unwavering love and support throughout this long process. Without Harsh's great sacrifices, I would not have been able to fulfill this dream of mine.

I would like to express the deepest appreciation to my committee chair Dr. A. Bruce Cahoon, who continually and convincingly conveyed a spirit of adventure in regard to research, and an excitement in regard to teaching. Without his guidance and persistent help this dissertation would not have been possible.

I would like to thank all my committee members and Ms. Joyce Miller, for their help and guidance. I would like to thank Middle Tennessee State University's Interdisciplinary Microanalysis and Imaging Center for donated time on the FIB-SEM apparatus, the Molecular Biosciences Program and the School of Graduate Studies for project support. I would also like to thank all my friends who supported me during my studies.

ABSTRACT

Plastids are a group of organelles present in the cells of higher and lower plants and algae. Along with photosynthesis, they provide a variety of biochemical capabilities and are one of the defining features of plant cells. These organelles are developmentally flexible and can convert from one type to another to accommodate for the physiological needs of a plant tissue. The presence and/or transitions from one plastid type to another are not well documented for all cases and the genetic and physiological basis of these transitions are not well understood. The goal for this study was to explore the plastids and their transitions in a single plant to better understand the underlying mechanisms of these changes and their overall effects on plant cells. As a consequence of this goal, I adapted a type of electron microscopy that had not been widely used on plant tissues, catalogued the organelles in each organ of *Arabidopsis thaliana*, and linked the chloroplasts leucoplast transition in petal cells to an amorphous aggregate seen in vacuoles.

Electron microscopy (EM) was the primary approach used in this dissertation. Transmission Electron Microscopy (TEM) was used to gain better knowledge of plastids. In addition, Focused Ion Beam Scanning Electron Microscopy (FIB-SEM) tomography was used, which offers the ability to produce serial slices of the materials (tissues) along with simultaneous SEM micrographs. The micrographs were used to create three dimensional (3D) renderings of the tissues with micron level resolution.

The successful application of FIB-SEM enabled the production of three dimensional renderings of five different tissues from *A. thaliana*: seed endosperm, leaf mesophyll, stem cortex, root cortex and petal lamina. The first part of this study

demonstrates the efficacy of this technique in plant tissue/cellular studies and its usefulness in studying organelle architecture and distribution.

The second part of this dissertation focuses on petal cells, specifically a structure present inside the petal vacuoles which has been overlooked or ignored in previous EM studies. This structure was found and named Petal Amorphous Aggregate (PAA) in the first part of this study. By utilizing TEM and FIB-SEM to explore the petal cell vacuoles of *A. thaliana*, *Brassica juncea* and *Cardamine bulbosa*, a link to the transition of chloroplasts to leucoplasts is made to PAA development. The micrographs obtained from TEM demonstrate the development of the PAA in a cell vacuole which I have defined in six stages. Micrographs also indicate the interaction between PAA and plastids during their transition from chloroplast to leucoplast and that these transitions are only present in white petal where these transitions occur.

TABLE OF CONTENTS

	Page
LIST OF FIGURES.....	ix
LIST OF ABBREVIATIONS.....	xi
CHAPTER ONE: INTRODUCTION.....	1
Plastids.....	1
FIB-SEM.....	6
Dissertation Structure.....	8
CHAPTER TWO: 3D PLANT CELL ARCHITECTURE OF ARABIDOPSIS THALIANA (BRASSICACEAE) USING FOCUSED ION BEAM-SCANNING ELECTRON MICROSCOPY.....	11
Abstract.....	12
Introduction.....	13
Materials and Methods.....	14
Results.....	17
Discussion.....	26
References.....	33

Appendices.....	36
Appendix A: Video of 3D reconstruction and rotation of (a) seed endosperm cells from the aleurone layer, (b) stem parenchymal cells, (c) root cortex cells, (d) leaf mesophyll cells, and (e) petal mesophyll cells..	37
Appendix B: Video of 3D ortho-rotation of (a) seed endosperm cells from the aleurone layer, (b) stem parenchymal cells, (c) root cortex cells, (d) leaf mesophyll cells, and (e) petal mesophyll cells.....	38
 CHAPTER THREE: PETAL CELL AMORPHOUS AGGREGATE DEVELOPMENT COINCIDES WITH THE CHLOROPLAST TO LEUCOPLAST TRANSITION.....	39
Abstract.....	40
Introduction.....	41
Materials and Methods.....	43
Results.....	46
Discussion.....	54
Conclusion.....	58
References.....	61
 CHAPTER FOUR: SURFACE DECONTAMINATION OF PLANT TISSUE EXPLANTS WITH CHLORINE DIOXIDE GAS.....	63
Abstract.....	64

Introduction.....	65
Materials and Methods.....	67
Results.....	69
Discussion.....	76
Conclusion.....	79
Acknowledgment.....	79
References.....	80
CONCLUSION.....	82
REFERENCES FOR INTRODUCTION AND CONCLUSION.....	84

LIST OF FIGURES

	Page
Figure 2.1: Five <i>Arabidopsis</i> tissues prepared for FIB-SEM sectioning and imaging....	19
Figure 2.2: High-resolution SEM micrographs from manual imaging.....	22
Figure 2.3: 3D renderings of the imaged areas of interest from the five tissues.....	24
Figure 2.4: 360° ortho-rotation for the five tissues.....	28
Figure 2.5: 3D false-colored volume rendering for the five cell types.....	30
Figure 3.1: FIB SEM sample preparation schematic.....	45
Figure 3.2: FIB SEM settings.....	45
Figure 3.3: Three regions of <i>A. thaliana</i> petal.....	47
Figure 3.4: TEM micrographs from three regions of an <i>A. thaliana</i> petal.....	48
Figure 3.5: TEM micrographs of plastid-PAA interaction.....	49
Figure 3.6: Orthographic projections of 3D reconstruction from three regions of <i>A. thaliana</i> petal tissue using FIB-SEM.....	51
Figure 3.7: TEM images from petal tips (P3 region) of <i>A. thaliana</i> , <i>B. juncea</i> and <i>C.</i> <i>bulbosa</i> flowers.....	53
Figure 3.8: Orthographic projection of 3D reconstructed blocks of petal tissue from <i>B.</i> <i>juncea</i> and <i>C. bulbosa</i> using FIB-SEM.....	55

Figure 3.9: Diagrammatic representation of six stages of a petal cell's life and PAA formation observed in <i>A. thaliana</i> petal.....	59
Figure 3.10: TEM micrographs of six stages of PAA development.....	60
Figure 4.1: Results of TSB assay showing inactivation of cauliflower curd surface microbioata using ClO ₂ gas generated with Fast Release powder.....	71
Figure 4.2: Impact of the most promising ClO ₂ gas treatments on elimination of viable microbioata and subsequent cauliflower curd explant viability.....	72
Figure 4.3: Tissue discoloration and viability after chlorine dioxide treatments.....	73
Figure 4.4: Shoot culture viability of cauliflower curd treated with ClO ₂ gas. Ten portions of cauliflower curd were cleaned with bleach.....	74

LIST OF ABBREVIATIONS

FIB – Focused Ion Beam

PAA – Petal Amorphous Aggregate

SEM – Scanning Electron Microscopy

TEM – Transmission Electron Microscopy

2D - Two Dimensional

3D - Three Dimensional

CHAPTER ONE

INTRODUCTION

PLASTIDS

Plastids are organelles essential for plant and algal life. They are double membrane-bound organelles that perform photosynthesis and a variety of metabolic reactions, including synthesis of fatty acids and secondary metabolites (Pyke, 2009). They proliferate via division of pre-existing organelles and are faithfully transmitted to daughter cells upon cell division, without *de novo* synthesis. Plastids are derived from proplastids (undifferentiated plastids) in the meristem of plant tissue and are categorized into a dozen distinct differentiated forms, such as chloroplasts (photosynthetic), chromoplasts (pigment-storing), etioplasts (present in senescing tissues), amyloplasts (starch-storing), leucoplasts (lacking plastids), and elaioplasts (lipid-storing), etc... corresponding to their cells or tissues type specific metabolic roles and appearance (Pyke, 2007; Pyke 2009). An interesting feature of plastids is that their development is controlled both by environmental signals and by intrinsic programs of cell differentiation. Most of these plastid forms are capable of being converted to chloroplasts upon light exposure (Pyke, 2009).

The ancestors of plastids were free-living prokaryotic cells related to cyanobacteria that were incorporated into a eukaryotic cell about 1.5 billion years ago (Hoffmeister and Martin, 2003). The conversion of a cyanobacterium to a plastid required several steps. There are several lines of evidence which indicate that chloroplasts in all

green plants and their non-photosynthetic relatives (plastids) are directly or indirectly derived from a single endosymbiotic event (Archibald, 2009). This original endosymbiosis of the cyanobacterium gave rise to plastids (primary plastids) in Archaeplastida, which are made up of Glaucophyta, Rhodophyta (red algae), and Viridiplantae (green algae and land plants). Four of the six eukaryotic subgroups possess plastids. This created a plant cell with three different sets of DNA, nuclear, mitochondrial and plastid (Sager and Ishida, 1963).

Over time, most of the genes that were once in the endosymbiont genome were either lost or transferred into host nuclear genome. Due to this, the size of the plastid genome has been reduced to one tenth that of the free living cyanobacterial genome (Archibald, 2009). This integration of prokaryotic genome into the nucleus of the eukaryotic cell is so extensive that the genetic material of plastids are now encoded by both nuclear and plastid genes, requiring coordination between the nucleus and the organelle for gene expression within the plastid (Pyke, 2009; Xin and Bhattacharya, 2010; Archibald, 2009).

The bulk of the plastid proteome consists of the nucleus encoded proteins that are translated on cytoplasmic ribosomes (Xin and Bhattacharya, 2010). A protein import apparatus was developed at the envelope membrane, in order to translocate proteins from cytoplasm to chloroplasts. There is no simple way to explain the gain and loss of plastids in all eukaryotes (Miyagishima, 2011). The origin of primary plastids via endosymbiosis involving a cyanobacterium is well-established, but the origin of secondary plastids is still controversial. In addition, subsequent tertiary endosymbioses involving other free-

living eukaryotes explain plastid origins in other eukaryote lineages (Xin and Bhattacharya, 2010; Miyagishma, 2011; Archibald, 2009).

All plastid types develop from embryonic and/or meristematic proplastids. Proplastids are undifferentiated double membrane organelles and are found at the tip of the shoots or roots, and also present in cultured plant cells and callus tissue. These are small about 1-2 μm in length, and contain little or no pigments (Pyke, 2009). They vary in number per cell at approximately 10-20 proplastids per cell. Proplastids divide by constriction in the centre of the plastid, and correct division of a proplastid is very crucial; failure to do so quickly leads to meristematic cells with no proplastids. This could lead to aplastidic cells, which would likely be lethal and meristem and organs derived from these cells will die quickly (Pyke, 1998). During cell division, proplastids are segregated relatively equally into the two daughter cells as a result of their even distribution in cell's cytoplasm, ensuring that a central plane of cell division will always result in proplastids in both daughter cells (Pyke, 2009). It may be that a more directed positioning of proplastids close to the nucleus and surrounding it, as directed by the cell's cytoskeleton is also possible, thereby also ensuring equality of segregation into the two newly formed cells (Pyke, 2009).

Another important aspect of proplastid biology is their role in plastid inheritance between generations. For most species plastids are maternally inherited but for others they are paternally or biparentally inherited (Pyke, 1998). In many species of angiosperms, proplastids are excluded from or degraded during pollen development, such that at fertilization, and the formation of a zygote, only proplastids from the maternal line

are present. Thus for the majority of angiosperms, plastids are maternally inherited but in about one-third of angiosperm species, some degree of biparental inheritance of plastids occur. In contrast, in the gymnosperms, the conifers show predominantly paternal plastid inheritance, whereas other gymnosperm groups are similar to angiosperms.

Chloroplasts are primarily chlorophyll containing plastids which are present in all green parts of the plant. Chloroplasts carry out the process of photosynthesis, and are by far the best understood plastid type in terms of their biochemistry and molecular biology (Lopez and Pyke, 2005). Leaves are the major sites for chloroplast development and accumulation, but they are also found in some other tissues, such as stems, petioles, pods, immature petals, sepals, tendrils etc... Their size varies between 5-10 μ m in length and 2-5 μ m in width (Pyke, 2009; Wise, 2006). In leaves of most plants the mesophyll cells contain approximately 50-200 chloroplasts (depending on the size of the cell and the chloroplast). Chloroplasts consist of an internal membrane system called thylakoid membranes, which form stacked arrangements called grana. A distinct compartment called the thylakoid lumen plays an important role in photosynthesis, especially in production of ATP (Pyke, 2009; Wise, 2006). In many plants, chloroplasts accumulate grains of starch as a product of photosynthesis during the day, which are broken down into sugars (maltose, maltodextrin, or hexose and triose phosphates), and exported to cytosol during the night, as the sugar concentration in cytosol is low due to inhibited cytosolic fructose synthesis. Chloroplasts can differentiate into different type of plastids, such as chromoplasts, amyloplasts, etioplasts or elaioplasts, mainly by virtue of changing

the type and extent of primary storage material (Pyke, 2009; Pyke, 1998; Lopez and Pyke, 2005).

Chromoplasts, are a specialized type of plastid that accumulates carotenoids, which are synthesized from the phytoene which is a dietetically valuable anti-oxidant found in many fruits and vegetables (Pyke, 2009; Wise, 2006). There are many different types and colors of carotenoids, e.g. carotenes are orange, lycopene is red and zeaxanthin and violoxanthin are yellow. These are responsible for final coloration in pigmented tissues, and are found in complexes on the thylakoid membrane of the chloroplasts, where they act as accessory pigments in light capture and energy dissipation by chlorophyll antenna complexes. Several of these are also found in thylakoid membrane and act as accessory pigments in light capture and energy dissipation by chlorophyll (Pyke, 2009; Wise, 2006). Carotenoids have been considered as valuable phytonutrients in food and have medical importance. Lycopene has been associated with prevention of cancer and cardiovascular diseases. Chromoplasts have been further categorized into five different categories, such as those which: a) are simple in structure, and contain globules of pigment accumulated in the stroma; b) contain distinct crystals, usually of lycopene or beta-carotene; c) contain extensive fibrillar or tubular structures; d) contain a complex network of twisted fibrils throughout the stroma; e) have extended concentric membranes (Pyke, 2009; Wise, 2006).

Elaioplasts are the specialized lipid-storing plastids. Lipids can be stored in special bodies within stroma named plastoglobules, these are relatively scarce in most plastids but in some circumstances, a significant number of plastoglobules accumulates in

elaioplasts. Elaioplasts are present in variety of tissues types such as, tapetal cells of the anthers in flowers, where lipid storage is required (Pyke, 2009; Lopez and Pyke, 2005). Some plants tissues require lipid for storage over starch for more efficient energy storage (e.g. seed endosperm), more accumulation of plastoglobuli takes place. Elaioplasts also contain several proteins including fibrillin, which forms a coat around the exterior of the postglobule, preventing them- from coalescing and remaining as a distinct entity. Plastoglobules are intimately connected with thylakoid membranes, so they should also be considered as stores of all molecules which play a role in the functionality of thylakoid membrane and which are exchangeable between the thylakoid plastoglobule compartments (Pyke, 2009; Lopez and Pyke, 2005).

Leucoplasts are colorless or non-pigmented plastids considered to be present in non-photosynthetic tissues and are observed in fully differentiated cells of petals, seed endosperm, stems and roots (Carde, 1984; Pyke, 2009). Leucoplasts are different from all other proplastids and every other plastid in structure and function. In comparison to chromoplasts, leucoplasts are much smaller in size and contain very little thylakoid membrane and some plastoglobuli. Although they lack pigments or storage materials, they play major and significant metabolic roles in these cells. They are the primary site of fatty acid, amino acid, and secondary metabolite synthesis, especially in roots (Pyke, 2009).

FIB-SEM

Over the past decades, several light and electron microscopy techniques have helped scientists study biological architecture at the tissue and cellular level in great

detail. For studies of plant structure, electron microscopy has been an important tool. Instead of using visible light the electron microscopes utilize focused electron beams and are capable of resolving much more defined details in comparison to the light microscope (Fowke, 1995). In the past, two types of electron microscopy have been used to study plant cells and tissues, transmission electron microscopy (TEM) that permits the study of internal features of cells and organelles in great details and the scanning electron microscopy (SEM) that can provide details about the external (surface) characteristics and morphology of intact cells and tissues (Fowke, 1995; Stokes et al., 2006). However, the need for true three dimensional imaging and desire to understand the 3D relationships of meso-scale hierarchies has led to the development of other advanced microscopy techniques. Several methods have been developed and used for 3D reconstruction of objects using series of images or 2D micrographs. The most intricate method among the methods used in past for 3D reconstruction is TEM tomography (Midgley and Weyland, 2003; Villinger et al., 2012)

TEM tomography requires a thin or semi-thin section that is projected in the electron beam to produce an image series which is then used for the virtual reconstruction of that section. With this method thin sections up to a thickness of $1\mu\text{m}$ can be successfully processed and reconstructed with outstanding resolution. However, to process samples thicker than $1\mu\text{m}$ requires serial sectioning of the samples. The procedure to obtain serial sections from a sample is technically challenging and complicated (Midgley and Wetland, 2003; Villinger et al., 2012).

An approach to overcome the demanding and cumbersome process of serial sectioning is FIB-SEM tomography. FIB-SEM is a type of electron microscopy that combines both slicing and imaging. This instrument uses a focused ion beam (FIB) that works at a nano scale and helps to reveal internal microstructure in a site specific manner. FIB-SEM is an instrument where SEM and FIB technologies have been brought together representing a powerful tool. FIB-SEM has been used for decades to study and verify three dimensional structures or architecture in material sciences (Sugiyama and Sigesato, 2004 ; Giannuzzi, 2005 ; Giannuzzi et al., 2005). This technique has recently been gaining wider use on the biological tissues (Merchán-Pérez et al., 2009 ; Bushby et al., 2011 ; Wei et al., 2012). A more detailed description of FIB-SEM and a survey of FIB-SEM literature can be found in the introduction of Chapter 2.

DISSERTATION STRUCTURE

The overall focus of this study is plastid presence and transitions in plant tissues and the use of FIB SEM to study these structures.

The first part of this study demonstrates the steps involved in the development of a FIB-SEM protocol for plant tissues. In order to do this, existing FIB-SEM protocols for animal tissues were modified and adjusted to produce 3D renderings of five tissues for *A. thaliana* (L.) Heynh. (root cortex, shoot cortex, seed aleurone, leaf mesophyll, and flower petal lamina). The results revealed good quality SEM micrographs, with easily identifiable sub-cellular architecture and organelles in all five tissue types, using FIB SEM, which proved that to obtain good quality micrographs modifications to the protocol were necessary. The 3D visualization of tissues gave a new insight of ultrastructural

organelles. Specifically, petal mesophyll cell that demonstrated an aggregate which had a regular crystalline-like structure and appeared to be present in the vacuoles of every cell in the visualized region (Bhawana et al., 2014).

The second part of this study focuses on the amorphous aggregate found in the petal mesophyll and epidermal cells. Previous studies of *A. thaliana* petals have noted electron dense vacuolar aggregate in petal mesophyll and epidermal cells but not considered it as any relevant structure (Weston and Pyke, 1999). 3D reconstructions and TEM micrographs of petal mesophyll and epidermal cells from three different species *A. thaliana*, *C. bulbosa* and *B. juncea* were used to test the hypothesis that these amorphous aggregates are the waste products produced when the plastids transition from the densely membranous chloroplast to the colorless leucoplasts in the flower petals. Results from this study describe the formation and degradation of the petal amorphous aggregates in *A. thaliana* and compares them to two other species.

Together, the results from these two studies provide a novel insight into organelles and possible mechanisms that have previously been ignored or were hard to be observed. The use of FIB-SEM for plant tissues and the 3D reconstructions proved to be useful in gaining new knowledge and better understanding of ultrastructural organelles.

The final chapter is a manuscript developed from a side-project that studied the efficacy of chlorine dioxide for tissue culture initiation. My work demonstrated that ClO₂ gas could be used in the preparation of plant tissues for micropropagation. The use of ClO₂ gas in that system decontaminated cauliflower curd surfaces at rates equal to bleach treatment but the ClO₂ treated tissues grew more quickly and were healthier than

the bleach treated samples. ClO₂ gas potentially represents an easy means to surface decontaminate plant tissues intended for micropropagation that when properly used does not pose a risk to human health.

CHAPTER TWO

3D PLANT CELL ARCHITECTURE OF ARABIDOPSIS THALIANA (BRASSICACEAE) USING FOCUSED ION BEAM-SCANNING ELECTRON MICROSCOPY

Bhawana, J. L. Miller and A. Bruce Cahoon

Published: Applications in Plant Sciences 2(6):1300090. 2014

ABSTRACT

Premise of the study: Focused ion beam–scanning electron microscopy (FIB-SEM) combines the ability to sequentially mill the sample surface and obtain SEM images that can be used to create 3D renderings with micron-level resolution. We have applied FIB-SEM to study *Arabidopsis* cell architecture. The goal was to determine the efficacy of this technique in plant tissue and cellular studies and to demonstrate its usefulness in studying cell and organelle architecture and distribution.

Methods: Seed aleurone, leaf mesophyll, stem cortex, root cortex, and petal lamina from *Arabidopsis* were fixed and embedded for electron microscopy using protocols developed for animal tissues and modified for use with plant cells. Each sample was sectioned using the FIB and imaged with SEM. These serial images were assembled to produce 3D renderings of each cell type.

Results: Organelles such as nuclei and chloroplasts were easily identifiable and other structures such as endoplasmic reticula, lipid bodies, and starch grains were distinguishable in each tissue.

Discussion: The application of FIB-SEM produced 3D renderings of five plant cell types and offered unique views of their shapes and internal content. These results demonstrate the usefulness of FIB-SEM for organelle distribution and cell architecture studies.

INTRODUCTION

There are several microscopy methods available to obtain intra- or subcellular structural information (Micheva and Smith, 2007; Helmstaedter et al., 2008; Lehrer, 2009 ; Wei et al., 2012). One of these techniques, focused ion beam–scanning electron microscopy (FIB-SEM), uses two beams: (1) a focused gallium ion beam and (2) an electron beam with secondary electron detector. The gallium beam can be used for imaging, can mill an area of interest to serially expose surfaces to reveal tissue and cell features, or can be used to produce high-quality sections of a sample for transmission electron microscopy (TEM) studies. The SEM beam can visualize an area of interest similar to conventional SEM. When combined, they enable a microscopist to section and visualize a sample with the same apparatus (Tanaka and Mitsushima, 1984; Heymann et al., 2006 ; Marko et al., 2007 ; Drobne et al., 2008 ; Knott et al., 2008 ; De Winter et al., 2009 ; Merchán-Pérez et al., 2009 ; Schneider et al., 2010 ; Bushby et al., 2011 ; Wei et al., 2012). This technique has been used in material science for decades (Sugiyama and Sigesato, 2004 ; Giannuzzi, 2005 ; Giannuzzi et al., 2005) but has recently been gaining wider use on biological tissues and is proving to be a powerful technology for creating 3D reconstructions of whole cells (Merchán-Pérez et al., 2009 ; Bushby et al., 2011 ; Wei et al., 2012). In terms of cost, FIB-SEM requires a dedicated apparatus that would require an investment comparable to a transmission electron microscope or access to a facility with an existing apparatus. The advantages of FIB-SEM over TEM tomography are (1) the ease of sectioning and image acquisition and (2) the chance of error during image realignment is minimized because serial images are acquired from a stationary block face. FIB-SEM has been used on biological tissues in two ways: (1) a sample may be embedded, sectioned,

and imaged using the FIB-SEM apparatus (Heymann et al., 2006); or (2) in some cases, the FIB capability is used to produce high-quality sections for TEM imaging (Wei et al., 2012). FIB-SEM has, to date, been used to produce three-dimensional renderings of animal cells (Bushby et al., 2011), microorganisms (Heymann et al., 2006; Wei et al., 2012), starch granules in plant cells (Crumpton-Taylor et al., 2012), and pollen cells (House and Balkwill, 2013).

Our objective for this study was to modify and apply existing FIB-SEM protocols developed for animal tissues to produce three-dimensional renderings of five tissues from *Arabidopsis thaliana* (L.) Heynh. (root cortex, shoot cortex, seed aleurone, leaf mesophyll, and flower petal lamina). We found that several modifications were necessary to achieve images of plant cells with FIB-SEM and that cells with dense cytoplasm (i.e., seed aleurone and root cortex cells) yielded the best results. We were able to easily identify subcellular architecture and organelles in all tissue types.

MATERIALS AND METHODS

Plant tissue and growth conditions

Arabidopsis thaliana was chosen for this study due to its small size, rapid growth cycle, and importance as a model plant system. Tissues were chosen in an attempt to survey a range of cellular content.

Root cortex tissues were obtained from 7–10-d-old seedlings grown on filter paper saturated with $1/2 \times$ Murashige and Skoog medium (Murashige and Skoog, 1962). Dry seeds were used as a source of aleurone tissue. Leaf mesophyll, stem cortex, and petal

lamina were obtained from 4–6-wk-old plants grown in potting soil at room temperature under fluorescent lights set on a 16 h light/8 h dark cycle.

Tissue fixation and preparation for FIB-SEM

A FIB-SEM protocol developed for animal tissues (Bushby et al., 2011) was the primary source for our methodology, with modifications based on Mikuła et al. (2004). FIB-SEM protocols for animal tissues have several modifications to the conventional fixation used in SEM or TEM methods, including en bloc staining using uranyl acetate (Heymann et al., 2006 ; Merchán-Pérez et al., 2009 ; Wei et al., 2012), prefixation in paraformaldehyde, and use of potassium ferricyanide and/or tannic acid to enhance the contrast (Knott et al., 2008 , 2011 ; Armer et al., 2009 ; De Winter et al., 2009 ; Hekking et al., 2009 ; Bushby et al., 2011 ; Wei et al., 2012).

Fresh tissue was cut into ~1-mm square or block portions and initially fixed in 2–3 mL of 2.5% glutaraldehyde (v/v) and 2.0% paraformaldehyde (w/v) in pH 7.3 0.1 M sodium cacodylate buffer for 2 h on a rotator. The primary fixative was removed, and the tissue samples were washed 2 × 10 min in 0.1 M sodium cacodylate buffer. Tissues were immersed in 2–3 mL of secondary fixative (1% osmium tetroxide [v/v], 1.5% potassium ferricyanide [w/v], in 0.1 M sodium cacodylate buffer) at room temperature for 2 h. The secondary fixative was removed, and tissues were washed 3 × 10 min with 0.1 M sodium cacodylate buffer. Buffer was replaced with 1% tannic acid (w/v) for 1 h and then removed by immersion in distilled water 3 × 10 min. Tissues were dehydrated by immersion in 30, 50, 70, 95, and 3 × 100% ethanol, for 10 min each, followed by 2 × 10 min in 100% propylene oxide (PO) (v/v). Subsequently, the tissues were immersed in 3 :

1 PO : Epon+Spurr for 1 h, 1 : 1 PO : Epon+Spurr for 1 h, 1 : 3 PO : Epon+Spurr overnight at room temperature, then 100% Epon+Spurr for 24 h (Mikuła et al., 2004). Fixed specimens were transferred into BEEM capsules (Ted Pella Inc., Redding, California, USA), oriented at the tip of the capsules, covered with 100% Epon+Spurr, and cured at 60 ° C for 24 h. The pyramidal ends of the plastic blocks were trimmed with a glass knife until tissue was reached. The area around the tissue was trimmed to form a trapezoid-shape measuring 0.5 mm × 1 mm (length × width). Each plastic block was immobilized with a vise, and a 4-mm portion containing the fixed tissue was removed using a fine hacksaw, forming a pyramid. The 4-mm pyramid was glued to a 12.5-mm aluminum SEM stub, using PELCO carbon tabs (Ted Pella Inc.), such that the imaging surface (the trapezoid) was horizontal to the stub surface. Each pyramid was coated with carbon glue excluding the trapezoidal surface. Finally, the pyramid was coated with a 200-nm layer of gold palladium using a Hummer 6.2 Sputtering Apparatus (Ladd Research Industries, Williston, Vermont, USA).

Focused Ion Beam-Scanning Electron Microscopy

The gold palladium-coated sample was placed on the specimen stage of the FIB-SEM apparatus and secured with the sample facing toward the outer edge of the vacuum chamber and the chamber pumped to high vacuum. When the SEM electron beam was engaged, the area of interest was identified using the secondary electron detector in a wide field. Next, the FIB high voltage and emission current were turned on and the FIB window opened. Sample working distance was set to 9 mm and the stage tilted to 55 °. FIB and SEM pictures were aligned using the FIB-SEM intersection (setting the eucentric position of the stage), and the magnification was set between 2500 × and 3000 × . A

platinum layer ($20\ \mu\text{m} \times 20\ \mu\text{m} \times 0.25\ \mu\text{m}$ [length \times width \times height]) was deposited on the area of interest. For milling, the ion beam current was initially set to 1000 pA but optimal beam current varied and was manually adjusted sample to sample. The regular cross-section feature and ion beam were used to mill a trench (FIB coarse trench milling) $20\ \mu\text{m} \times 20\ \mu\text{m} \times 10\ \mu\text{m}$ to expose the targeted area. Fine milling and the polishing feature were used to remove debris or imperfections from the front face of the platinum-coated area (targeted area). The block face was automatically or manually sliced using the FIB slicing + SEM image acquisition feature, with a thickness of 100 nm for each slice and 10 ns/slice dwell time.

Image processing

Images were processed using ImageJ (Schneider et al., 2012). Briefly, the area of interest was selected within the image frame and cropped. Brightness and/or contrast were adjusted and the processed images saved in TIFF format. ImageJ 3D viewer was used to compile the stack into a three-dimensional rendering, make orthogonal slices or 3D rotations, or save images in .avi format to be viewed as a movie.

RESULTS

Five different tissues were explored using FIB-SEM. Areas of interest included seed aleurone (Figure 2.1a), stem cortex (Figure 2.1d), root cortex (Figure 2.1g), leaf mesophyll (Figure 2.1j), and petal mesophyll (Figure 2.1m). A $20 \times 20 \times 0.25\ \mu\text{m}$ platinum layer was placed on each area of interest (Figure 2.1b, e, h, k, n) to protect it from burning (or destruction) by the FIB beam as well as to provide a leveled surface for even slicing. A trench was

milled around each platinum layer to expose the targeted area (block face) for sectioning and imaging (Figure 2.1c, f, i, l, o). Automated serial sectioning and imaging of seed aleurone cells provided 90 micrographs by serially removing 100-nm sections from the block face. Some manual images were also collected (Figure 2.2a–c). Automated images were assembled to obtain a three-dimensional reconstruction, 360 ° orthogonal rotation (Figs. 2.3a, 2.4a ; Videos 2.1a, 2.2a), and a three-dimensional false-colored volume rendering of the tissue (Figure 2.5a). Stem cortex cells adjacent to the epidermis and extending toward the vascular bundle were automatically sectioned and imaged to produce 141 micrographs. Several high-resolution manual images were also collected (Figure 2.2d–f). Micrographs from serial sectioning were used to produce a three-dimensional reconstruction, 360 ° orthogonal rotation, and three-dimensional false-colored volume rendering for the stem tissue (Figures. 2.3b, 2.4b, 2.5b ; Videos 2.1b, 2.2b).

Automated serial sectioning and imaging of root endodermis and cortex tissue yielded 88 micrographs. Manual images were also collected (Figure 2.2g–i). Sections were assembled to produce a three-dimensional reconstruction (Figure 2.3c, Video 2.1c), 360 ° orthogonal rotation (Figure 2.4c, Appendix A), and three-dimensional false-colored volume rendering of the tissue (Figure 2.5c).

Leaf mesophyll cells were automatically sectioned and imaged to yield 141 micrographs. Manual images were also collected (Figure 2.2j–l). Serial sections were used to produce a three-dimensional reconstruction, 360 ° orthogonal rotation, and three-dimensional false colored volume renderings of the tissue (Figure 2.3d, 2.4d, 2.5d; video 2.1d, 2.2d). Petal mesophyll cells were automatically sectioned and imaged to yield 142 micrographs.

Manual images were also collected (Figure 2.2 m–o). Sections were used to produce a three-dimensional reconstruction, 360 ° orthogonal rotation, and three-dimensional false-colored volume rendering of the tissue (Figures 2.3e, 2.4e, 2.5e; Appendix B)

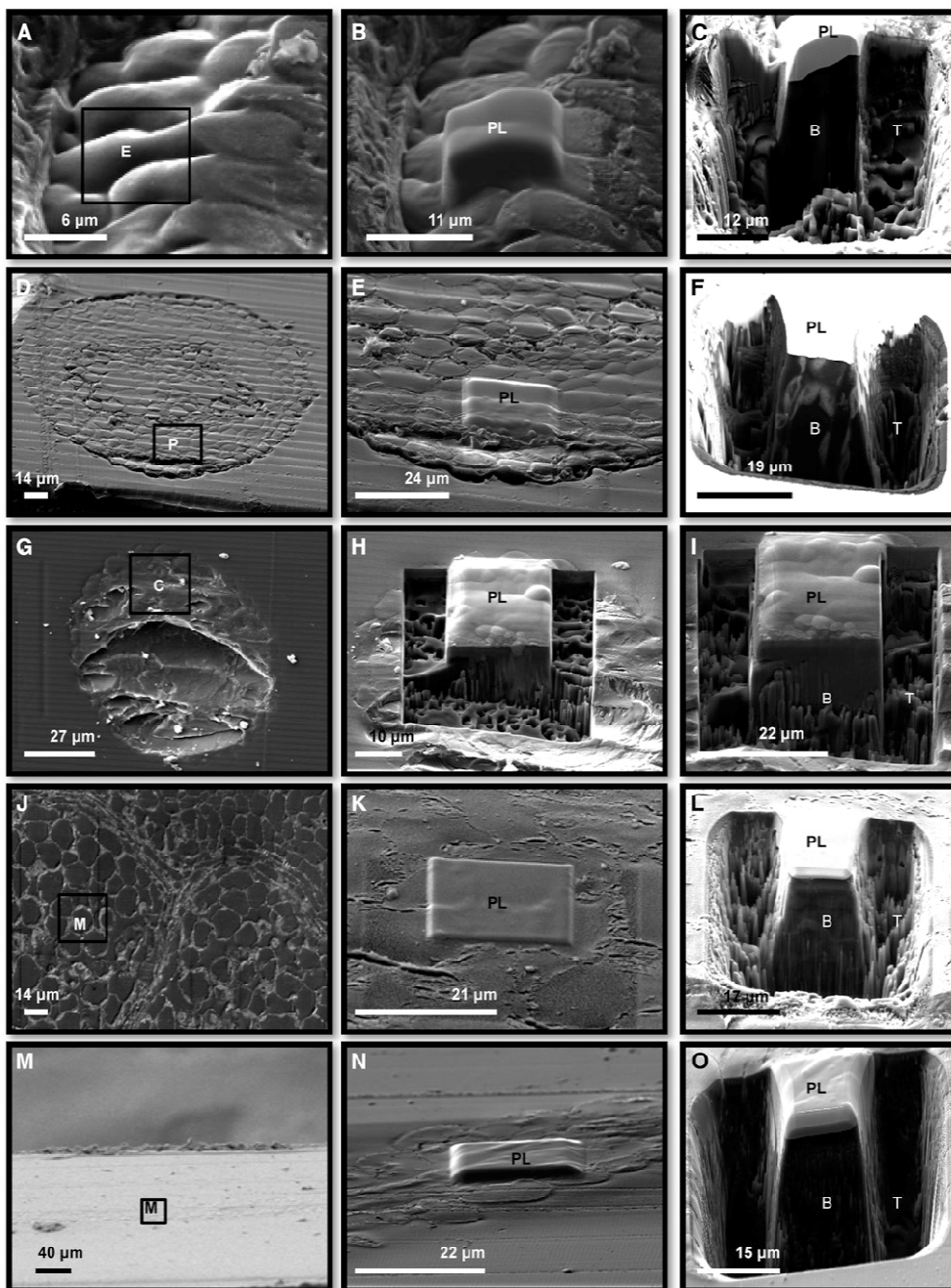


Figure 2.1: Five *Arabidopsis* tissues prepared for FIB-SEM sectioning and imaging.

Stages of the FIB-SEM process are demonstrated, including choosing an area of interest, depositing a platinum layer (PL), and milling to create a block for serial sectioning. Dry seeds were fixed, sliced, and imaged for aleurone visualization (a–c): (a) the endosperm cells (E)* of the aleurone area of interest viewed at a 55 ° angle; (b) a 250-nm platinum layer (PL) applied to the area of interest; (c) a U-shaped trench (T) was milled with the gallium ion beam around the area of interest to expose a block face (B) for sectioning and imaging. Stem tissue (d–f): (d) whole stem transverse section showing parenchymal (P)* cells; (e) a 250-nm platinum layer (PL) was placed on an area of interest across the cortex spanning from the first layer of parenchymal cells interior to the epidermis to the endodermis; (f) a milled trench (T) at the area of interest, the first parenchymal layer is visible on the block face (B). Root tissue (g–i): (g) cortex cells (C)* of a whole root transverse section from the elongation zone shown at a 0 ° angle; (h) a 250-nm platinum layer (PL) was placed on the cortex extending from the endodermis toward the epidermis, and a trench was partially milled, shown at a 55 ° angle; (i) the completed trench (T) showing an exposed block surface. Leaf tissue (j–l): (j) mesophyll cells (M)* were chosen as the area of interest, shown here at a 0 ° angle of a transverse section; (k) a 250-nm platinum layer (PL) on the area of interest (mesophyll cells); (l) a trench (T) was milled exposing the block face (B). White petals from fully opened flowers (m–o): (m) the faint outline of a petal transverse section is shown at a 55 ° angle (mesophyll cells [M]* were chosen for imaging); (n) a 250-nm platinum layer (PL) was placed on the area of interest; (o) a trench (T) was milled, exposing the block surface. Abbreviations: B =

block face; C = cortex cells; E = endosperm cells; M = mesophyll cells; P = parenchymal cells; PL = platinum layer; T = trench. *Squares in a, d, g, j, and m represent the areas of interest for each tissue.

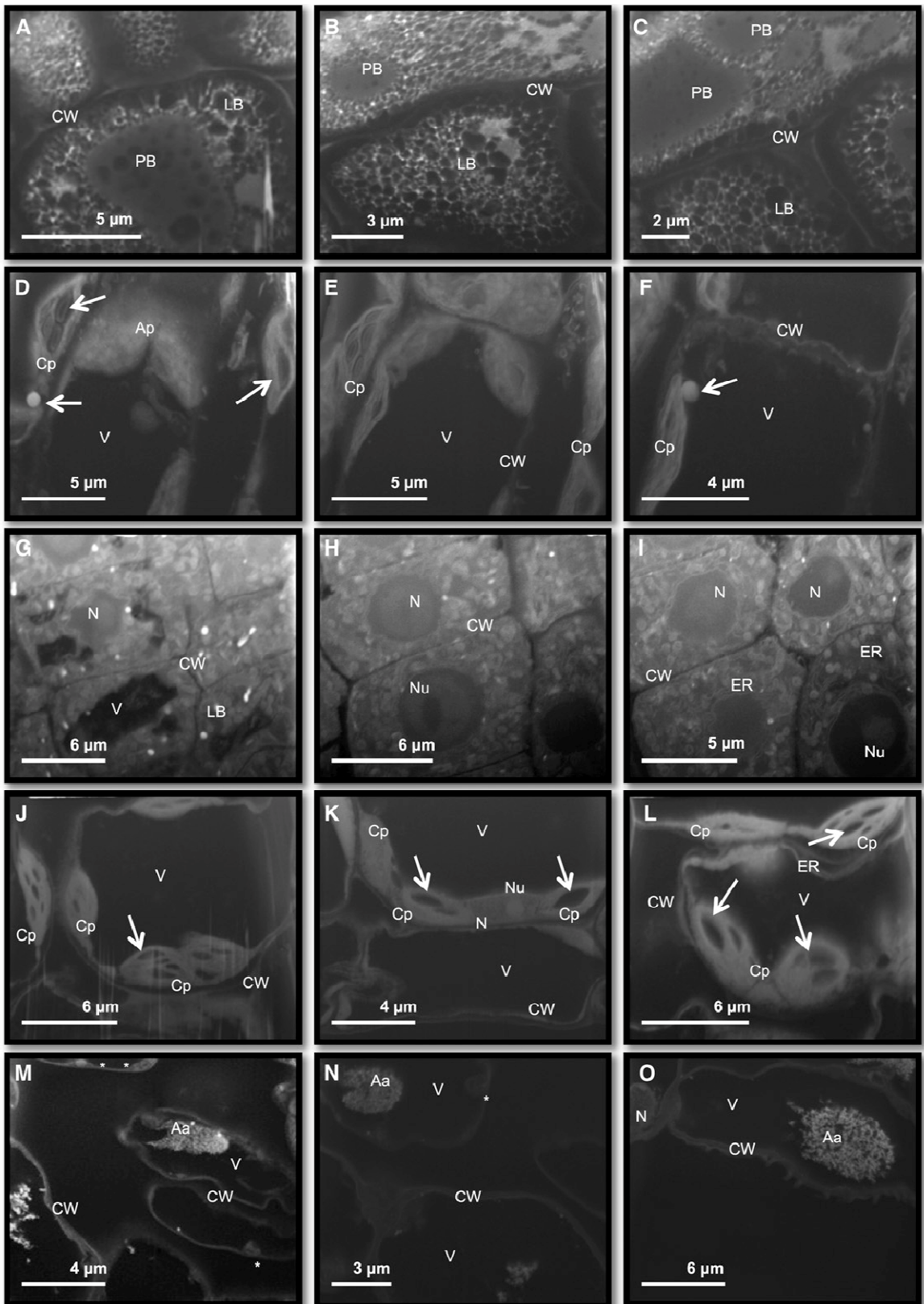


Figure 2.2: High-resolution SEM micrographs from manual imaging. At least 40 images were collected from each cell type in this study. Three representative images from each cell type are shown and subcellular bodies labeled to demonstrate the resolution achieved. (a–c): Seed aleurone cells showing protein bodies (PB), lipid bodies (LB), and cell walls (CW). (d–f): Stem cortex cells showing chloroplasts (Cp), amyloplast (Ap), starch grains (arrows), cell wall (CW), and vacuoles (V). (g–i): Root cortex cells showing vacuole (V), nucleus (N), nucleolus (Nu), lipid bodies (LB), cell wall (CW), and endoplasmic reticulum (ER). (j–l): Leaf mesophyll cells showing chloroplasts (Cp) and internal membranous endoplasmic reticulum connections (ER). (m–o): Petal mesophyll cell showing nucleus (N), vacuoles (V) and amorphous aggregate (Aa), cell wall (CW), and some organelles (*) with details below the lower limit of the resolution of this technique. Abbreviations: Aa = amorphous aggregate; Ap = amyloplast; Cp = chloroplast; CW = cell wall; ER = endoplasmic reticulum; LB = lipid body; N = nucleus; Nu = nucleolus; PB = protein body; V = vacuole.

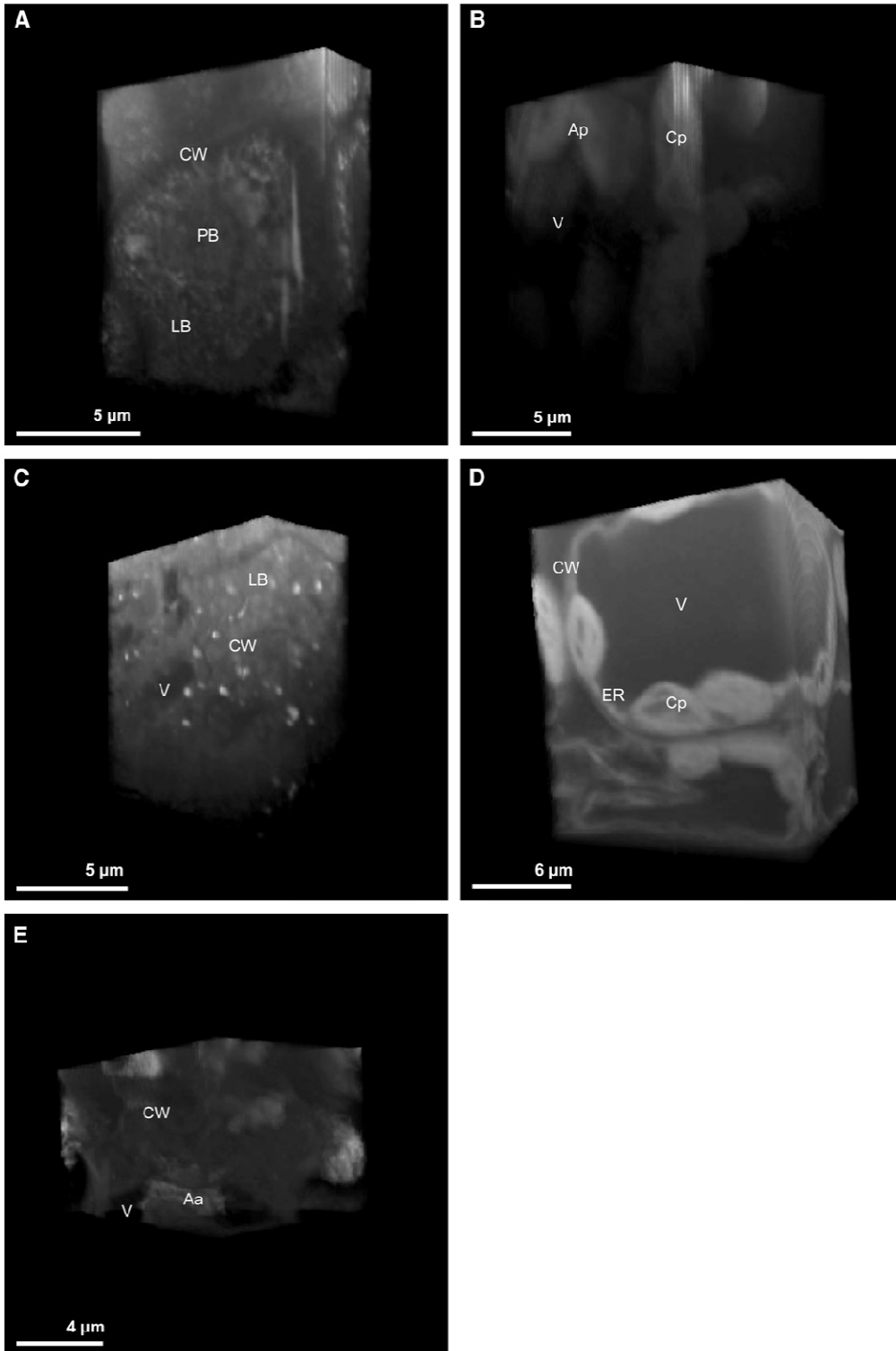


Figure 2.3: 3D renderings of the imaged areas of interest from the five tissues. Serial images were assembled to create 3D renderings of each cell type. Approximate blocks of dimensions $20 \times 20 \times 10 \mu\text{m}$ were imaged and visualized using FIB-SEM, and the images were used to create a 3D rendering with ImageJ. (a) Seed aleurone cells, (b) stem cortex, (c) root cortex, (d) leaf mesophyll, (e) petal mesophyll. Abbreviations: Aa = amorphous aggregate; Ap = amyloplast; Cp = chloroplast; CW = cell wall; ER = endoplasmic reticulum; LB = lipid body; PB = protein body; V = vacuole.

DISCUSSION

Plant cell and tissue tomography has been possible for sometime (Pellegrini, 1980), but recent improvements and accessibility in computational methodologies and image manipulation have greatly decreased the labor necessary to produce images and have increased the range of applications. For example, X-ray tomography allows imaging of whole plant organs (Mairhofer et al., 2012), and TEM tomography allows the detailed visualization of subcellular structures (Austin and Staehelin, 2011). FIB-SEM enables imaging of structures between the resolution capabilities of TEM and X-ray tomographies. It has proven useful in plant studies for the visualization and distribution of starch grains (Crumpton-Taylor et al., 2012) and pollen anatomy (House and Balkwill, 2013).

The goal of this study was to modify FIB-SEM protocols developed for animal tissues, determine the efficacy of FIB- SEM in plant tissue and/or cellular studies, and demonstrate its usefulness in studying organelle architecture and distribution. A successful survey of five plant tissues was completed using the modified protocol, and 3D reconstructions were produced that provided visualization of plant cells at a unique resolution.

In the seed aleurone layer, 2D micrographs and a 3D reconstruction of the aleurone cells revealed irregularly shaped cells with densely packed cytoplasm. There were numerous protein bodies and lipid bodies, and well-defined cell walls were easily identifiable and comparable to organelle images in micrographs from TEM studies on endosperm and embryo cells of *Daucus carota* L. seed (Dawidowicz-Grzegorzewska, 1997) and perisperm and endosperm of *Phelipanche aegyptiaca* (Pers.) Pomel seed (Joel et al.,

2012). Stem 2D micrographs and 3D renderings of fixed stem tissue revealed highly vacuolated elongated collenchyma cells with fully developed chloroplasts and starch grains very similar to those seen in micrographs of leaf blades of *Arabidopsis* (Musgrave et al., 1998). Amyloplasts and the cell walls were also identifiable and comparable to those in micrographs of meristem cells in *D. carota* embryo (Dawidowicz Grzegorzewska, 1997) and endosperm cells of *Arundo formosana* Hack. (Jane, 1999). Root micrographs and 3D reconstruction of root cells revealed columns of regular block-shaped cells with dense cytoplasm, a prominent nucleus, nucleolus, cell wall, and vacuoles. Subcellular structures were identifiable and comparable to those in published micrographs for *Glycine max* (L.) Merr. root cells (Yu et al., 2011) and cortical cells of *Cucumis sativus* L. root (Lee et al., 2002). Lipid bodies and starch grains were identifiable and comparable to those seen in micrographs for *A. formosana* endosperm cells (Jane, 1999) and *D. carota* (Dawidowicz- Grzegorzewska, 1997). Membranes adjacent to the nucleus and throughout the cells were similar to endoplasmic reticulum found in root meristematic cells of *Allium sativum* L. (Jiang and Liu, 2010) and cortical cells of *C. sativus* root (Lee et al., 2002).

Leaf 2D images and 3D renderings of fixed leaf mesophyll cells produced by FIB-SEM allowed the visualization of cellular and subcellular features and provided a view of chloroplast distribution that was unique, but also consistent with previously published 2D electron micrographs (Musgrave et al., 1998). Cell shape was generally oblate and circular, with relatively thin cell walls. Chloroplasts with low-resolution thylakoid stacks were also clearly identifiable as were nuclei, starch grains, and internal cytoplasmic membranes.

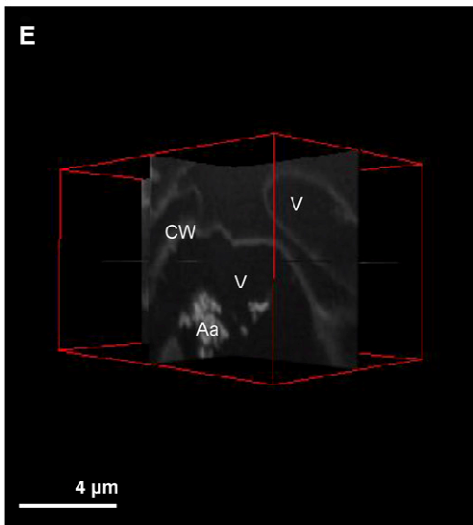
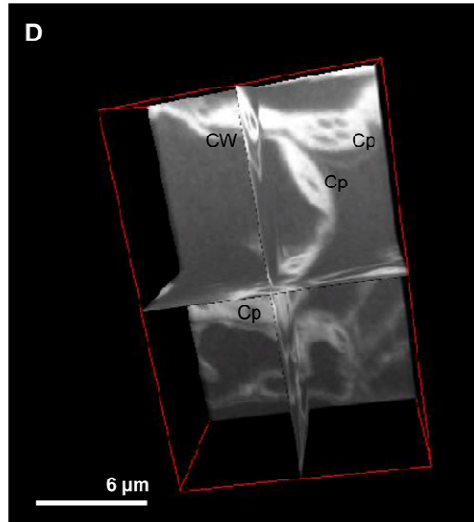
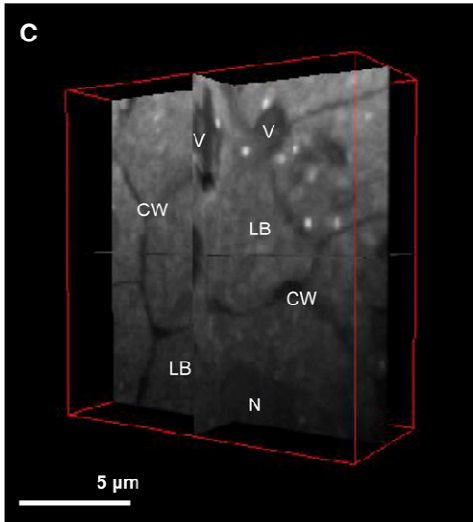
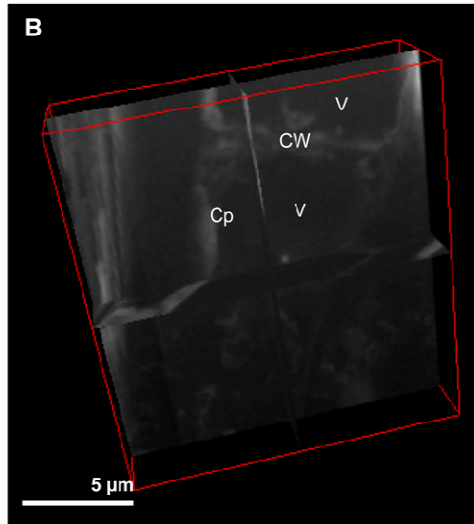
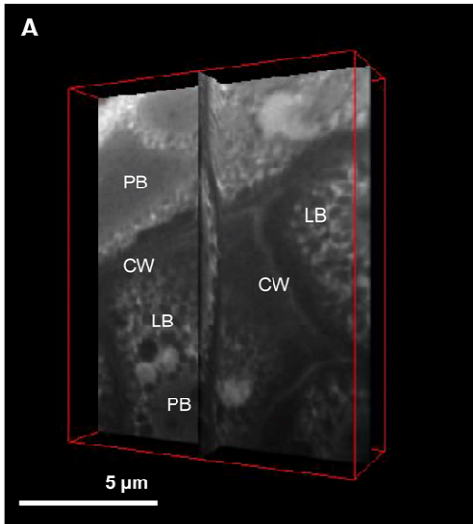


Figure 2.4: 360° ortho-rotation for the five tissues. 360° ortho-rotations were created to demonstrate the ability to visualize interior planar sections from the 3D reconstructions.

(a) Seed aleurone cells, (b) stem cortex, (c) root cortex, (d) leaf mesophyll, (e) petal mesophyll. Abbreviations: Aa = amorphous aggregate; Cp = chloroplast; CW = cell wall; LB = lipid body; PB = protein body; V = vacuole.

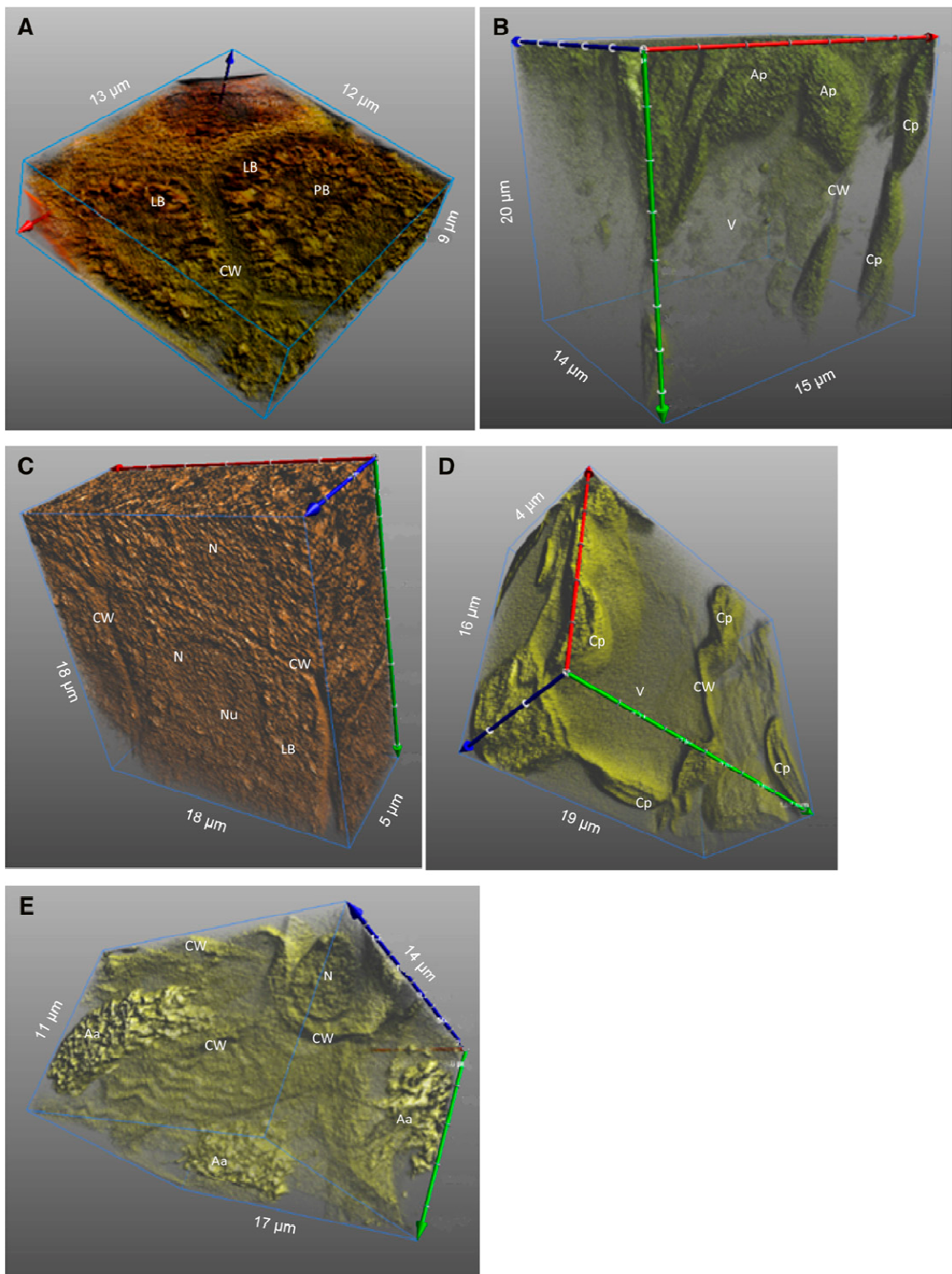


Figure 2.5: 3D false-colored volume rendering for the five cell types. False-coloring was manually added to 3D reconstructions to add greater contrast to some of the prominent structures. (a) Seed aleurone cells, (b) stem cortex to parenchymal cells, (c) root endodermis to cortex cells, (d) leaf mesophyll cells, (e) petal mesophyll cells. Axes are color coded: x = red, y = green, z = blue. Abbreviations: Aa = amorphous aggregate; Ap = amyloplast; Cp = chloroplast; CW = cell wall; LB = lipid body; N = nucleus; Nu = nucleolus; PB = protein body; V = vacuole.

Petal mesophyll 2D images and 3D renderings revealed elongated, irregularly shaped cells arranged into aerenchymous tissue as previously reported for *Arabidopsis* (Pyke and Page, 1998) and numerous other species (Kay et al., 1981). Cells were highly vacuolated similar to those of another member of the Brassicaceae, *Erysimum cheiri* (L.) Crantz (Weston and Pyke, 1999). Published transmission electron micrographs of *Arabidopsis* white petal mesophyll have shown electron-dense leucoplasts in the thin strip of cytoplasm typical for these cells (Pyke and Page, 1998). There were several structures that may have been mitochondria, leucoplasts, or large vesicles, but the SEM images obtained in this study lacked the resolution to definitively identify them. Inside the petal mesophyll cell vacuoles, an amorphous aggregate was clearly visible in 3D reconstructions. This feature has been mentioned in 2D TEM studies as an electron opaque material in the mesophyll and epidermal cell vacuoles of *Erysimum* petals (Weston and Pyke, 1999), but its presence in those images was relatively unremarkable.

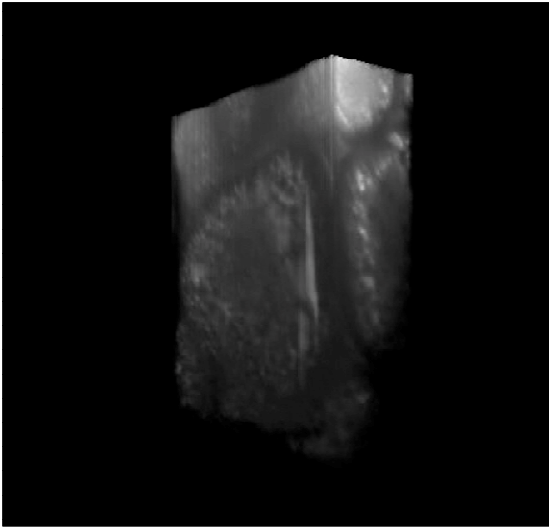
REFERENCES

- Armer HEJ, Mariggi G, Png KMY et al. Imaging transient blood vessel fusion events in Zebrafish by correlative volume electron microscopy. *PLOS ONE*. 2009. 4, e7716.
- Austin JR, Staehelin LA. Three-dimensional architecture of grana and stroma thylakoids of higher plants as determined by electron tomography. *Plant Physiology*. 2011;155:1601-1611.
- Bushby AJ, P'ng KMY, Young RD, Pinali C, Knupp C, Quantock AJ. Imaging three-dimensional tissue architectures by focused ion beam scanning electron microscopy. *Nature Protocols*. 2011; 6:845–858.
- Crumpton-Taylor M, Grandison S, Png KMY, Bushby AJ, Smith AM. Control of starch granule numbers in Arabidopsis chloroplasts. *Plant Physiology*. 2012;158:905–916.
- Dawidowicz-Grzegorzewska A. Ultrastructure of Carrot Seeds during matricconditioning with micro-cel E. *Annals of Botany*. 1997;79:535–545.
- De Winter DAM, Schneijdenberg CTWM, Lebbink MN et al. Tomography of insulating biological and geological materials using focused ion beam (FIB) sectioning and low-kV BSE imaging. *Journal of Microscopy*. 2009;233:372–383.
- Drobne D, Milani M, Leser V et al. Imaging of intracellular spherical lamellar structures and tissue gross morphology by a focused ion beam/scanning electron microscope (FIB/SEM). *Ultramicroscopy*. 2008;108:663–670.
- Giannuzzi LA. *Introduction to focused ion beams: Instrumentation, Theory, Techniques and Practice*, Springer, New York, New York, USA; 2005.
- Giannuzzi LA, Kempshall BW, Schwarz SM, Lomness JK, Prenitzer BI, Stevie FA. FIB lift-out specimen preparation techniques. In *Introduction to focused ion beams*, L.A. Giannuzzi, and F.A. Stevie, eds., 201–228. Springer, New York, New York, USA; 2005.
- Hekking LHP, Lebbink MN, De Winter DAM et al. Focused ion beam-scanning electron microscope: exploring large volumes of atherosclerotic tissue. *Journal of Microscopy*. 2009;235:336–347.
- Helmstaedter M, Briggman KL, Denk W. 3D structural imaging of the brain with photons and electrons. *Current Opinion in Neurobiology*. 2008;18:633–641.
- Heymann JAW, Hayles M, Gestmann I, Giannuzzi LA, Lich B, Subramaniam S. Site-specific 3D imaging of cells and tissues with a dual beam microscope. *Journal of Structural Biology*. 2006;155:63–73.
- House A, Balkwill K. FIB-SEM: An additional technique for investigating internal structure of pollen walls. *Microscopy and Microanalysis*. 2013;19:1535-1541.

- Jane W. Ultrastructure of embryo development in *Arundo formosana* Hack. (Poaceae). *International Journal of Plant Sciences*. 1999;160:46–63.
- Jiang W, Liu D. Pb-induced cellular defense system in the root meristematic cells of *Allium sativum* L. *BMC Plant Biology*. 2010;10:40.
- Joel DM, Bar H, Mayer AM et al. Seed ultrastructure and water absorption pathway of the root-parasitic plant *Phelipanche aegyptiaca* (Orobanchaceae). *Annals of Botany*. 2012;109:181-195.
- Kay QON, Daoud HS, Srirton CH. Pigment distribution, light reflection and cell structure in petals. *Botanical Journal of the Linnean Society*. 1981;83:57-83.
- Knott G, Marchman H, Wall D, Lich B. Serial section scanning electron microscopy of adult brain tissue using focused ion beam milling. *The Journal of Neurosciences*. 2008;28:2959–2964.
- Knott G, Rosset S, Cantoni M. Focused ion beam milling and scanning electron microscopy of brain tissue. *Journal of Visualized Experiments*. 2011;53:2588.
- Lee SH, Singh AP, Chung GC, Kim YS, Kong IB. Chilling root temperature causes rapid ultrastructural changes in cortical cells of cucumber (*Cucumis sativus* L.) root tips. *Journal of Experimental Botany*. 2002;53:2225–2237.
- Lehrer J. Neuroscience: Making connections. *Nature News*. 2009;457:524–527.
- Mairhofer S, Zappala S, Tracy SR et al. RooTrak: Automated recovery of three-dimensional plant root architecture in soil from X-Ray microcomputed tomography images using visual tracking. *Plant Physiology*. 2012;158:561-569.
- Marko M, Hsieh C, Schalek R, Frank J, Mannella C. Focused-ion-beam thinning of frozen-hydrated biological specimens for cryo-electron microscopy. *Nature Methods*. 2007;4:215–217.
- Merchan-Perez A, Rodriguez JR, Alonso-Nanclares L, Schertel A, DeFelipe J. Counting synapses using FIB/SEM microscopy: A true revolution for ultrastructural volume reconstruction. *Frontiers in Neuroanatomy*. 2009;3:18.
- Micheva KD, Smith SJ. Array tomography: a new tool for imaging the molecular architecture and ultrastructure of neural circuits. *Neuron*. 2007;55:25–36.
- Mikuła A, Tykarska T, Zielinska M, Kuras M, Rybczynski JJ. Ultrastructural changes in zygotic embryos of *Gentiana punctata* L. during callus formation and somatic embryogenesis. *Acta Biologica Craconiensia Series Botanica*. 2004;46:109–120.
- Murashige T, Skoog F. A revised medium for rapid growth and bio assays with Tobacco tissue cultures. *Physiologia Plantarum*. 1962;15:473–497.

- Musgrave ME, Kuang A, Brown CS, Matthews SW. Changes in Arabidopsis leaf ultrastructure, chlorophyll and carbohydrate content during spaceflight depend on ventilation. *Annals of Botany*. 1998;81:503–512.
- Pelligrini M. Three-dimensional reconstruction of organelles in *Euglena gracilis* Z. *Journal of Cell Science*. 1980;43:137-166.
- Pyke KA, Page AM. Plastid ontogeny during petal development in Arabidopsis. *Plant Physiology*. 1998;116:797-803.
- Schneider CA, Rasband WS, Eliceiri KW. NIH Image to ImageJ: 25 years of image analysis. *Nature Methods*. 2012;9:671–675.
- Schneider G, Guttman P, Heim S et al. Three-dimensional cellular ultrastructure resolved by X-ray microscopy. *Nature Methods*. 2010;7:985–987.
- Sugiyama M, Sigesato G. A review of focused ion beam technology and its applications in transmission electron microscopy. *Journal of Electron Microscopy*. 2004;53:527–536.
- Tanaka K, Mitsushima A. A preparation method for observing intracellular structures by scanning electron microscopy. *Journal of Microscopy*. 1984;133:213–222.
- Wei D, Jacobs S, Modla S et al. High-resolution three-dimensional reconstruction of a whole yeast cell using focused-ion beam scanning electron microscopy. *BioTechniques*. 2012;53:41–48.
- Weston EL, Pyke KA. Developmental ultrastructure of cells and plastids in the petals of Wallflower (*Erysimum cheiri*). *Annals of Botany*. 1999;84:763–769.
- Yu HN, Liu P, Wang ZY, Chen WR, Xu GD. The effect of aluminium treatments on the root growth and cell ultrastructure of two soybean genotypes. *Crop Protection (Guildford, Surrey)*. 2011;30:323-328.

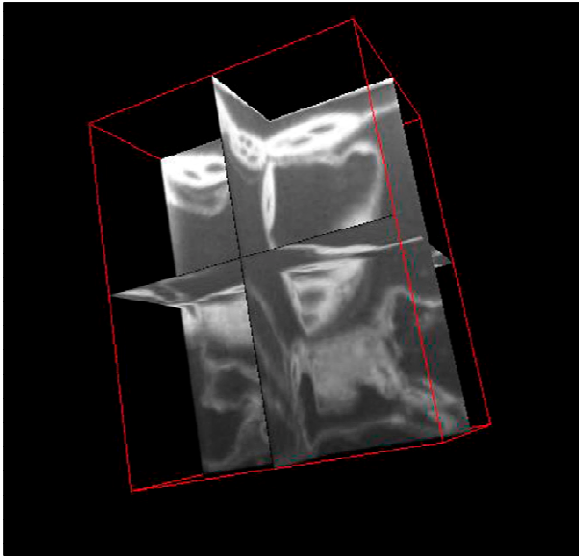
APPENDICES



Appendix A. Video of 3D reconstruction and rotation of (a) seed endosperm cells from the aleurone layer, (b) stem parenchymal cells, (c) root cortex cells, (d) leaf mesophyll cells, and (e) petal mesophyll cells. Micrographs were collected by milling fixed tissue accompanied by SEM imaging using FIB-SEM.

This video is Windows Media (.wmv) file and can be viewed here with QuickTime or Windows Media Player, or can be viewed from the Botanical Society of America's YouTube channel.

<http://www.youtube.com/watch?v=0nnqMBJILA0>



Appendix B. Video of 3D ortho-rotation of (a) seed endosperm cells from the aleurone layer, (b) stem parenchymal cells, (c) root cortex cells, (d) leaf mesophyll cells, and (e) petal mesophyll cells. Micrographs were collected by milling fixed tissue accompanied by SEM imaging using FIB-SEM. This video is Windows Media (.wmv) file and can be viewed here with Quick- Time or Windows Media Player, or can be viewed from the Botanical Society of America's YouTube channel.

<http://www.youtube.com/watch?v=B3tEY8X85f4>

CHAPTER THREE

**PETAL CELL AMORPHOUS AGGREGATE DEVELOPMENT
COINCIDES WITH THE CHLOROPLAST TO LEUCOPLAST
TRANSITION**

Bhawana and A. Bruce Cahoon

Submitted to: Protoplasma

October, 2014.

ABSTRACT

Flower petal mesophyll and epidermal cell vacuoles of *Arabidopsis thaliana* have an undefined amorphous aggregate. These crystalline-looking structures have not been seen in other tissues of this species or other species which raises the question of its origin and/or function in petal development. *Arabidopsis* petal cells begin their development as green tissues that transition to white upon flower maturation. The petals undergo programmed cell death after pollination and nutrients are recycled. We hypothesized that the amorphous aggregates are an intermediary structure formed from the waste materials generated during the transition of chloroplasts to leucoplasts during petal cell development. From our data we show that petal amorphous aggregates (PAA) appear in the vacuoles of *Arabidopsis* petals during/after the transition from green to a white tissue and were able to define six stages of petal cell and PAA development. We also show that PAAs are present in two white-flowered self-pollinating members of the Brassicaceae family, *A. thaliana* and *Cardamine bulbosa* but are absent in the yellow flowered *Brassica juncea*.

INTRODUCTION

Arabidopsis petals are distinctive simple laminar organs; the white petal blades are relatively large and spoon shaped and lack chlorophyll. These petals possess a morphology similar to other broad and flat plant organs but with unusual conical epidermal cells on their adaxial surface at maturity (Mara et al., 2010; Irish, 2010). Unlike similarly shaped organs, such as leaves, *Arabidopsis* petals have a well defined very short life span which has very likely been influenced by the predominance of self-pollination (Droon, 1997).

All petals are considered to be modified leaves pre-programmed to senesce after its reproductive role is complete. Some petals, including *Arabidopsis*, begin development as green organs containing chloroplasts. As the petal expands and matures these chloroplasts lose both chlorophyll, and thylakoid membranes to become leucoplasts in white, pink or blue flowers or chromoplasts in yellow, orange or red colored flowers (Whatley, 1984; Thomas et al., 2003). These changes remain stable to maintain petal colors until pollination occurs or the flower is aborted. Post-pollination, whole petals senesce, cellular constituents are degraded, and nutrients are remobilized. This remobilization of mineral nutrients is primarily nitrogen and phosphorous from the petals and is believed to contribute either to the development of the ovary or to that of new flowers (Kenichi et al., 2013; Thomas et al., 2003; Jones, 2013).

The cellular mechanism of petal senescence is still unclear. Biochemical studies of leaf senescence have shown that the thylakoid pigment protein complex is disassembled and chlorophyll is broken down into phytol, magnesium and water soluble cleavage products,

which are removed and stored in vacuoles (Martinoia et al., 2000). Autophagy is considered to play a role in nutrient relocalization during leaf senescence. Several electron microscopy studies demonstrate autophagy occurs during petal senescence and show vesicles budding into the vacuoles presumably carrying cytoplasmic components. However, it is unknown if this is the cause of cell death or a mechanism of efficient remobilization of nutrients (Jones, 2013; Avila-Ospina et al., 2014; Matile and Winkenbach, 1971).

Once petal senescence is complete, dramatic autophagic activities of the large central vacuole can be observed in all cells. Decaying cytoplasmic organelles (mitochondria, ribosomes etc) appear to be transported into the vacuole by invaginations of the tonoplast where the cytoplasmic material becomes exposed to the lysosomal enzymes. In some cells autophagic activities last until only a very thin layer of cytoplasm is left behind (Matile and Winkenbach, 1971).

One study of *Arabidopsis* has noted an electron dense vacuolar aggregate in petal mesophyll and epidermal cells (Weston and Pyke, 1999). A recent 3-D visualization of petal mesophyll cells demonstrated that this aggregate had a regular crystalline-looking structure and appeared to be present in the vacuoles of every cell in the visualized region (Bhawana et al., 2014). This structure was coined a petal amorphous aggregate (PAA) as it was not seen in any other tissues in the *Arabidopsis* plant. In this study we test the hypothesis that these amorphous aggregates are vacuole targeted waste products produced when densely membranous chloroplasts transition to colorless leucoplasts in the flower petals. We use transmission electron microscopy (TEM) and focused ion beam

scanning electron microscopy (FIB-SEM) to describe the formation of the PAA in *Arabidopsis* cells and compare them to petals from two other members of the Brassicaceae family – *Brassica juncea* and *Cardamine bulbosa*.

MATERIALS AND METHODS

Tissue collection

Arabidopsis thaliana and *Brassica juncea* (var. Southern Giant Mustard) were grown in an incubator at 28°C with a 16 hr light/8 hr dark cycle. *Cardamine bulbosa* flowers were field collected on the MTSU campus in April 2014. *A. thaliana* flower petals were collected between developmental stages 13 and 15 (Smyth et al., 1990). *B. juncea* petals were collected from fresh, fully opened flowers on 6-8 week old plants. *C. bulbosa* petals were collected from fresh fully opened flowers.

Tissue preparation for TEM and FIB-SEM

Individual petals from each species were collected from fully open flowers and initially fixed in 2-3 ml of 2.5% glutaraldehyde (v/v) and 2.0% paraformaldehyde (w/v) in pH 7.3 0.1 M sodium cacodylate buffer for 2 hr on a rotator. The primary fixative was removed and the tissue samples were washed 2 x 10 min in 0.1M sodium cacodylate buffer.

Tissues were immersed in 2-3 ml of secondary fixative (1% osmium tetroxide (v/v), 1.5 % potassium ferricyanide (w/v), in 0.1M sodium cacodylate buffer) at room temperature for 2hr. The secondary fixative was removed and tissues were washed 3 x 10 min with 0.1M sodium cacodylate buffer. Buffer was replaced with 1% tannic acid (w/v) for 1 hr

and then removed by immersion in distilled water 3 x10 min. Tissues were dehydrated by immersion in 30, 50, 70, 95 and 3 x100% ethanol, for 10 min each, followed by 2 x 10 min in 100% propylene oxide (PO) (v/v). Subsequently the tissues were immersed in 3:1 PO:Epon+Spurr resin for 1 hr, 1:1 PO and Epon+Spurr for 1 hr, 1:3 PO:Epon+Spurr overnight at room temperature, then 100% Epon+Spurr for 24 hr (Mikula et al., 2004). Fixed specimens were transferred into flat embedding molds, oriented at the tip, and covered with 100% Epon+Spurr, and cured at 60°C for 24 hr.

For TEM, fixed specimens (flat capsules) were trimmed and thin sectioning was done using glass knives (prepared using Leica EM KMR2 Knife-maker) for each tissue to obtain multiple sections of approximately 60-100nm using a Leica Ultracut UCT Microtome. These sections were collected on a copper grid and stained using uranyl acetate and Sato's lead. Sections were observed and imaged with a Hitachi H-7650-II Transmission Electron Microscope at 10kv.

For FIB-SEM, the ends of the fixed specimens (flat capsules) were trimmed to 1x1mm trapezoids and reduced in height to about 4mm. These specimens were carbon taped on SEM specimen mounts and coated with carbon glue. A 200nm layer of gold-palladium was placed on these samples using Hummer 6.2 Sputtering Apparatus. Once coated these samples were further processed (milled, polished, sectioned and imaged) using a Tescan Lyra 3 Focused Ion Beam Field Emission Scanning Electron Microscope.

A diagrammatic representation of the FIB-SEM process is presented in Figure 3.1 and instrument settings are shown in Figure 3.2.

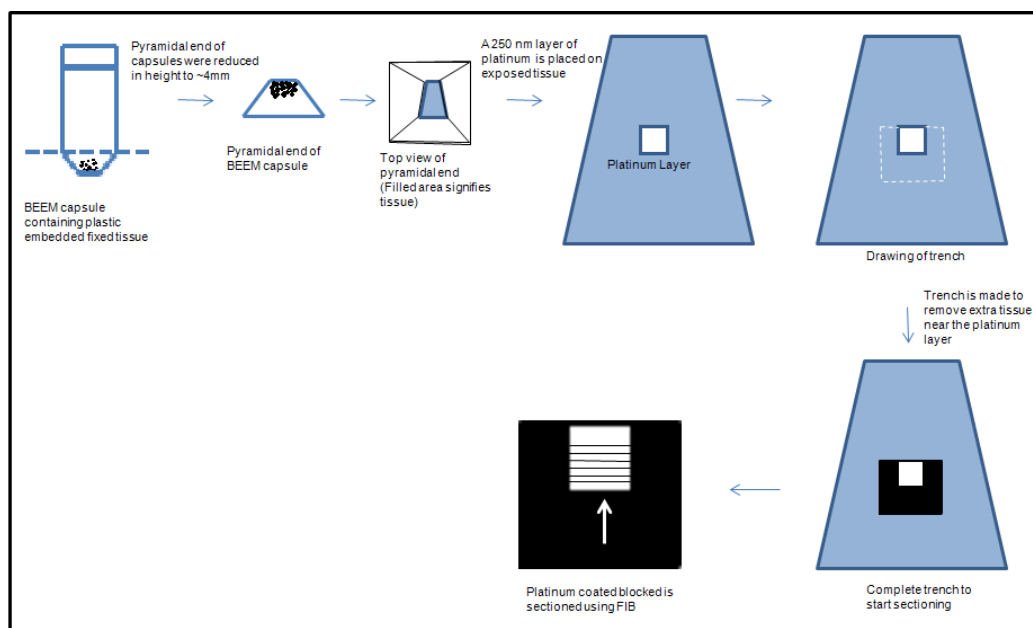


Figure 3.1: FIB-SEM sample preparation schematic, showing the process of block preparation, platinum layer deposition and ablation with FIB.

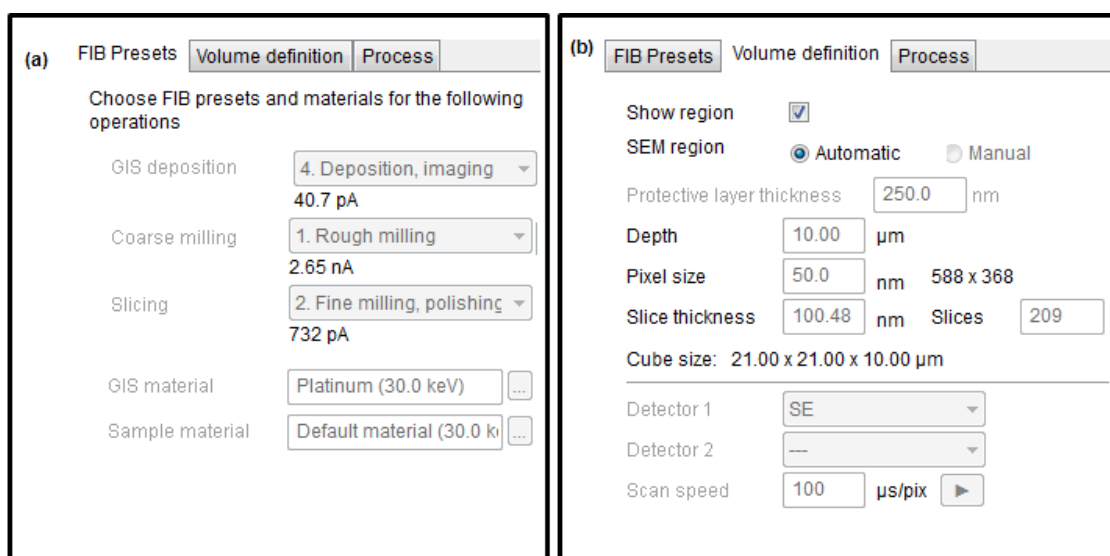


Figure 3.2: FIB SEM settings for a) Platinum deposition, trench milling and slicing, b) Volume definition.

RESULTS

PAA Development in *A. thaliana*

The presence of PAAs in *Arabidopsis* petals was determined using TEM and FIB-SEM methodologies to visualize the internal anatomy of cells. Individual petals from *Arabidopsis* were divided into three regions - the P1 petal base tissues were green and represented the least developed petal cells, the P2 mid region represents a transition between the green base and the white tip, and the P3 petal tip represents the oldest cells in the petal (Figure 3.3).

Mesophyll, abaxial or adaxial epidermal petal cells were chosen as areas of interest within each region. TEM micrographs revealed that mesophyll cells in the green P1 base of the petal had a disorganized array of electron dense material inside the vacuoles, no obvious tonoplast invaginations, and intact chloroplasts (Figure 3.4 a-d). Mesophyll cells in the P2 middle portion of the petal had organized PAAs in some of the cells, obvious invaginations in the tonoplasts indicative of vacuolar transport, reduced chloroplasts, and leucoplasts (Figure 3.4 e-h). Mesophyll and adaxial epidermal cells in the P3 tip portion of the petal had well-organized PAAs, tonoplast invaginations (detailed image in Figure 3.5), leucoplasts, and no intact chloroplasts (Figure 3.4 i-l). Cells in the P3 region were also found where the tonoplast had ruptured and the cell was dead (Figure 3.4j). PAAs were often located directly across the tonoplast from a transitioning plastid (Figure 3.5).

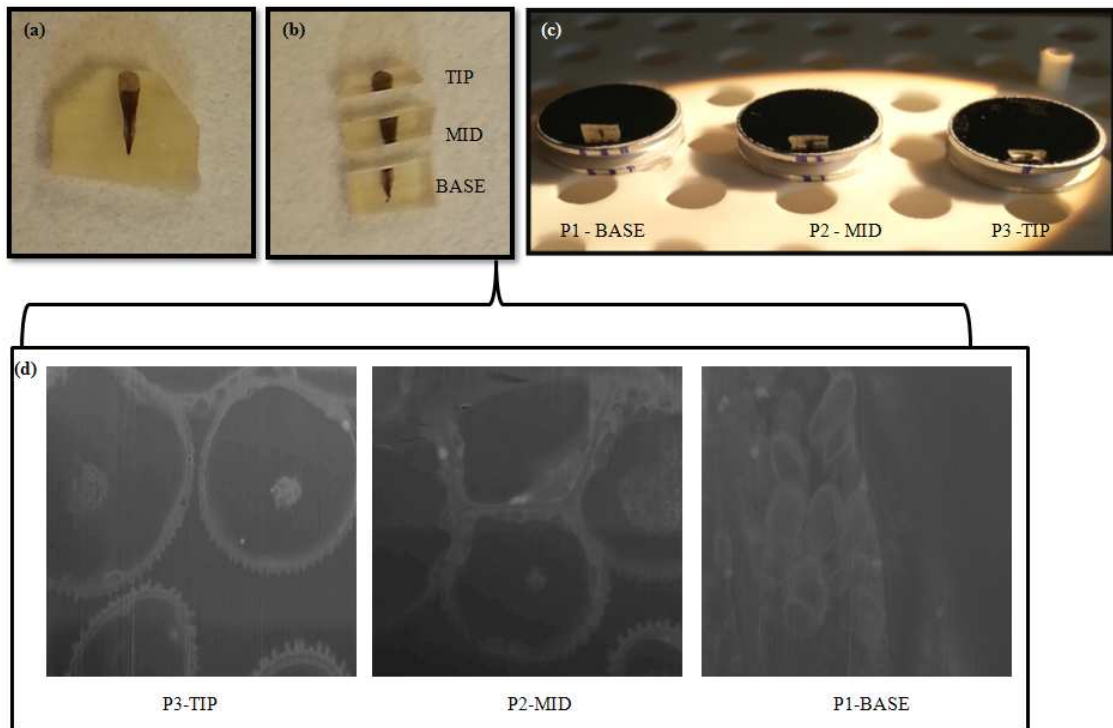


Figure 3.3: Three regions of *A. thaliana* petal

- a) Whole fixed petal in resin, b) Petal dissected into three regions, P1- Base of petal, P2 – Middle of petal and P3 – Tip of petal c) Blocks with each petal portion mounted on stubs and d) TEM micrographs from P1, P2 and P3 region.

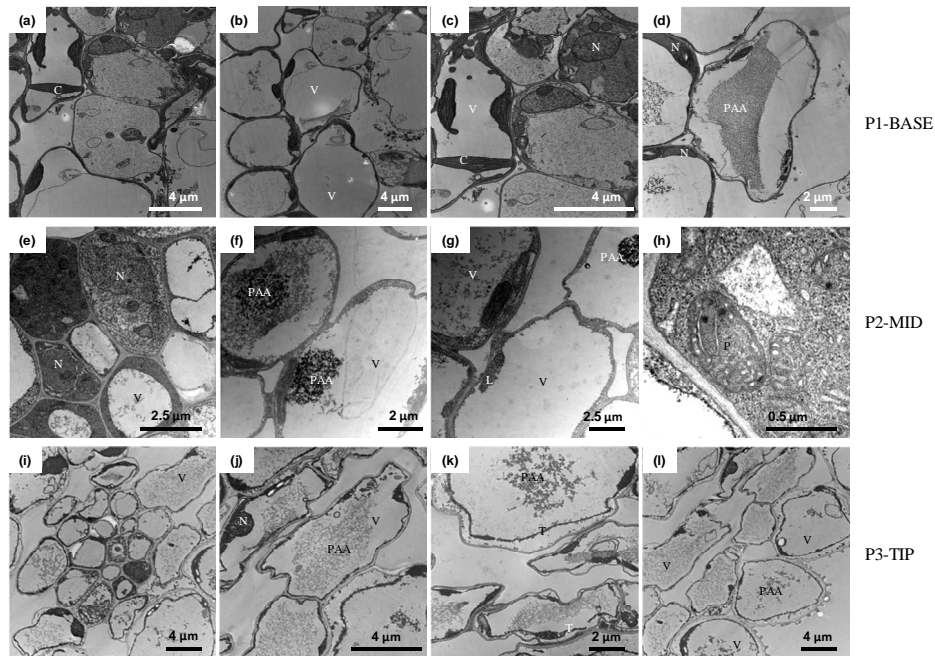


Figure 3.4: TEM micrographs from three regions of an *A. thaliana* petal.

(a – d): Four micrographs from the P1 region (base of petal), showing various cells with intact chloroplast (C), vacuoles (V), and disorganized PAAs.

(e – h): Four micrographs from P2 region (mid-section of the petal), showing cells undergoing chloroplast to leucoplast (L) transition, cells with large amounts of cytoplasmic content with visible nuclei (N), and formation of well defined PAAs.

(i – l): Four micrographs of cells in the P3 region (petal tip), where the majority of the cells are mature and/or dying, have minimal cytoplasmic content due to ruptured tonoplasts (T), have completed chloroplast to leucoplast transition, and less defined PAAs.

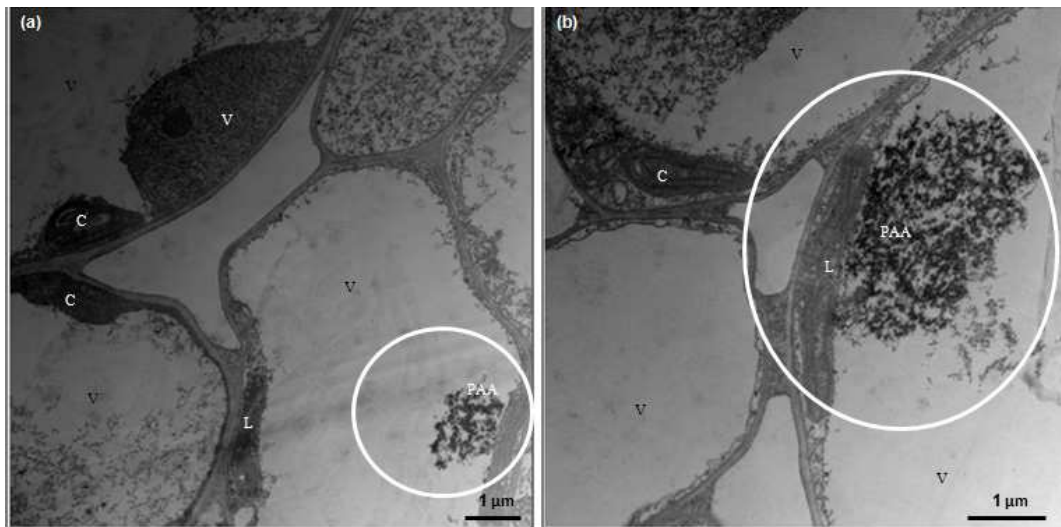


Figure 3.5: TEM micrographs of plastid-PAA interaction

(a – b) Cells showing plastids and PAA located directly across the tonoplast from each other. The interaction is highlighted in a circle.

In each section cells were seen in varying stages of development indicating that transitions were not progressing at uniform rates for adjacent cells. For example in the base region, most cells had obvious chloroplasts but some had begun the process of degradation while others had not. In the mid-section, PAA size and development varied significantly. In the tip region some cells were viable while some had a ruptured tonoplast membrane.

FIB-SEM was used to section through entire cells to confirm that TEM results were accurate, that no features were missed due to sectioning, and that the observed phenomena were not artifacts of staining. An average of 100 SEM micrographs were collected for each tissue. 3-D reconstruction for the three regions of *Arabidopsis* petal confirmed trafficking of cytoplasmic content and formation of AAs in the central vacuoles of P3 and P2 regions and the absence of AA and trafficking in the P1 region (Figures 3.6 a-f and Video 1).

Overall, these three regions differ in the size of vacuole, number of chloroplasts and leucoplasts present and also in the developmental stages of individual cells. The P1 region had more chloroplasts in comparison to other two regions and AAs were absent in this region.

PAA in other members of the Brassicaceae

Petals from *A. thaliana*, *B. juncea*, and *C. bulbosa* were compared to explore the structure and formation of PAAs in the central vacuole.

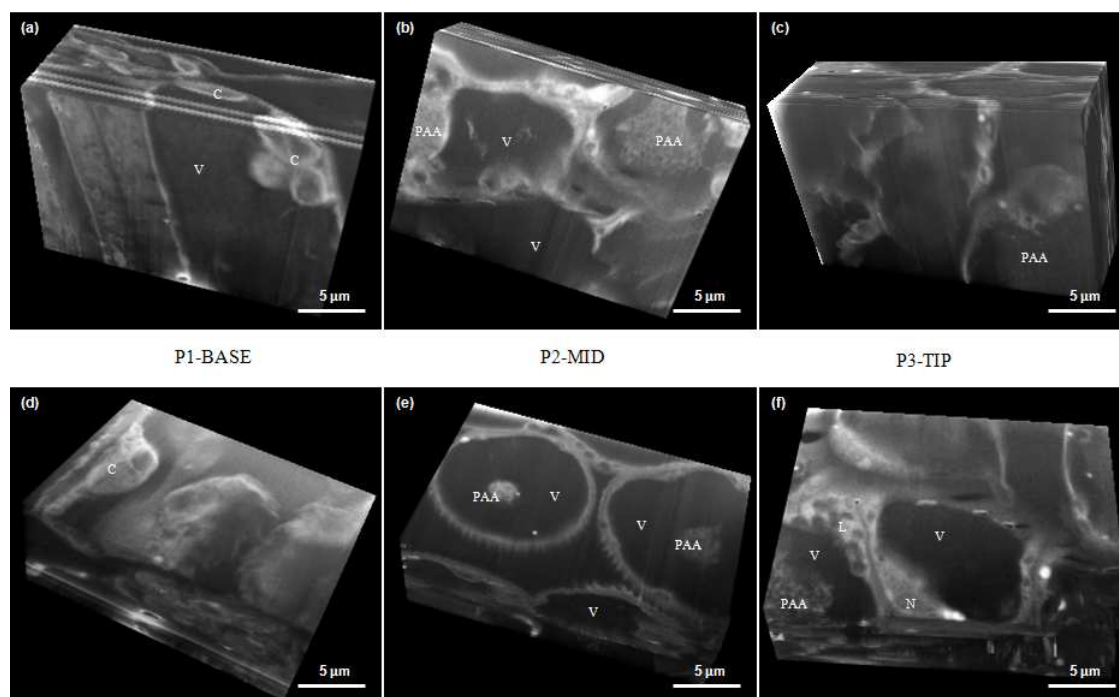


Figure 3.6: Orthographic projections of 3D reconstruction from three regions of *A. thaliana* petal tissue using FIB-SEM.

(a-c): Front of the reconstructed block showing the P1(mesophyll cells), P2(abaxial epidermal cells) and P3(adaxial epidermal cells) regions.

(d-f): Back of the reconstructed block showing the P1(adaxial epidermal cells), P2(adaxial epidermal cells) and P3(mesophyll cells) regions.

Videos of each are available as P1P2P3- 3D reconstruction and rotation. Video 1:

https://www.youtube.com/watch?v=sxFOMUystrI&list=UU1u_lj0_RaWmJEwens0yBaQ

These three plants were chosen because they belong to the Brassicacea family and could be used to challenge the hypothesis that the vacuolar PAA is formed as a by-product during the transition of chloroplasts to leucoplasts in white petal cells. *C. bulbosa* has white petals with a green base and is primarily self-pollinated similar to *A. thaliana*. *B. juncea* has yellow flowers with chromoplasts that do not have a green base.

TEM images of yellow petal cells from *B. juncea* revealed disorganized electron dense particles in the vacuoles of mesophyll and epidermal cells (Figures 3.7 e-h) but no PAAs. The disorganized particles seen throughout the petals of *B. juncea* are also visible in some portions of *A. thaliana* and *C. bulbosa* petals (Figure 3.7 a, e and l) TEM images from white *C. bulbosa* petals revealed PAA-like structures in the vacuoles of mesophyll and epidermal cells (Figures 3.7 i-l) somewhat similar to those seen in the P2 and P3 portions of *A. thaliana*. Ruptured tonoplasts were also visible in the *C. bulbosa* cells (Figure 3.7k).

FIB-SEM was used to make 3D reconstructions of the mesophyll and epidermal cells from *C. bulbosa*, and *B. juncea*. An average of 100 SEM images or micrographs were used for each reconstruction. The structures noticed or absent in *C. bulbosa*, and *B. juncea* were confirmed with the 3D renderings (Figures 3.8a-d, Videos 2 a-b).

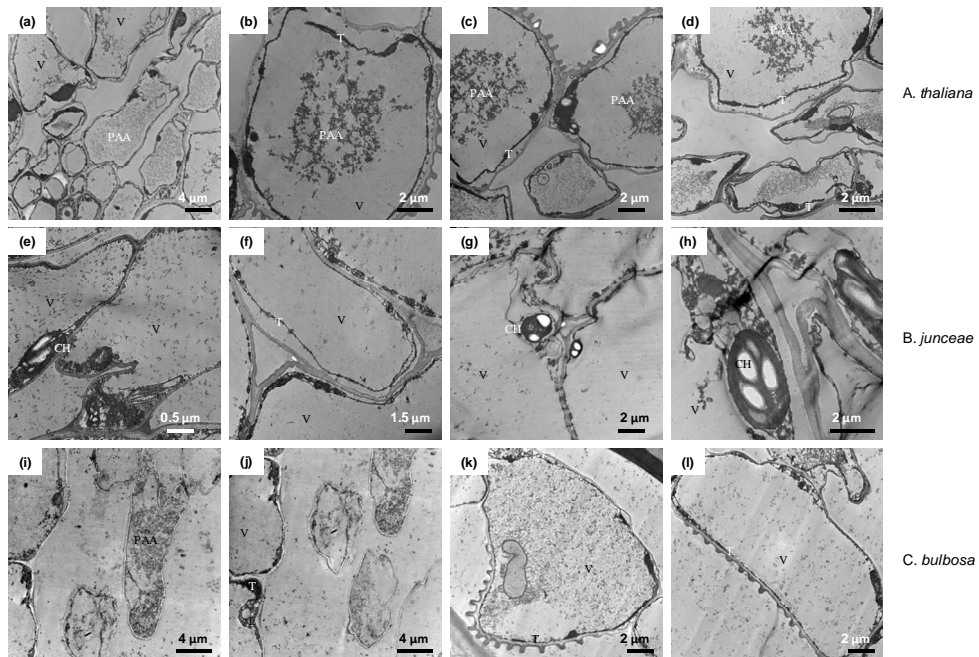


Figure 3.7: TEM images from petal tips (P3 region) of *A. thaliana*, *B. juncea* and *C. bulbosa* flowers.

(a – d): Four groups of cells from an *A. thaliana* petal showing intact well defined PAAs, poorly defined PAA's, and cells with broken tonoplasts.

(e – h): Cells from *B. juncea* petal showing amyloplast, mitochondria, intact tonoplast and vacuoles with no PAA's.

(i – l): Cells from *C. bulbosa* showing, leucoplasts, vacuolar trafficking of cytoplasmic content and some PAA-like formations.

DISCUSSION

Vacuoles are present in all plant cells but differ in form and function (Swanson et al., 1998). Historically, vacuoles are considered a temporary storage site for waste or protein and other nutrients which may play important role in plant growth and development. In recent years vacuoles have been recognized as multipurpose organelles that carry out numerous metabolic functions (Echeverria, 2000; Shumway et al., 1972).

Vacuoles have a large number of different hydrolases and hence are known to have lysosomal character (Hortensteiner and Feller, 2002). They play an important role in cell development and senescence by providing defense against biotic and abiotic damage, accumulation of metabolites and autolysis. These three key roles are important for cell viability, pollination and cell death (Thomas et al., 2003). The sequestration of pigments and catabolites in the vacuoles is considered an adaptation for protection against photodamage (Thomas et al., 2003; Matile and Hortensteiner, 1999).

The color of reproductive structures like petals and fruits is considered to be a result of carotenoid accumulation or accumulation of vacuolar anthocyanins, especially in flowers. These accumulations are typically observed to occur before senescence or in some cases are associated with the reproductive phase of a flower's life (Thomas et al., 2003). In this study we followed the development of colorless PAAs in white flowers of *A. thaliana*. It is known that *A. thaliana* petals are green as immature buds, but they become white as they expand and mature.

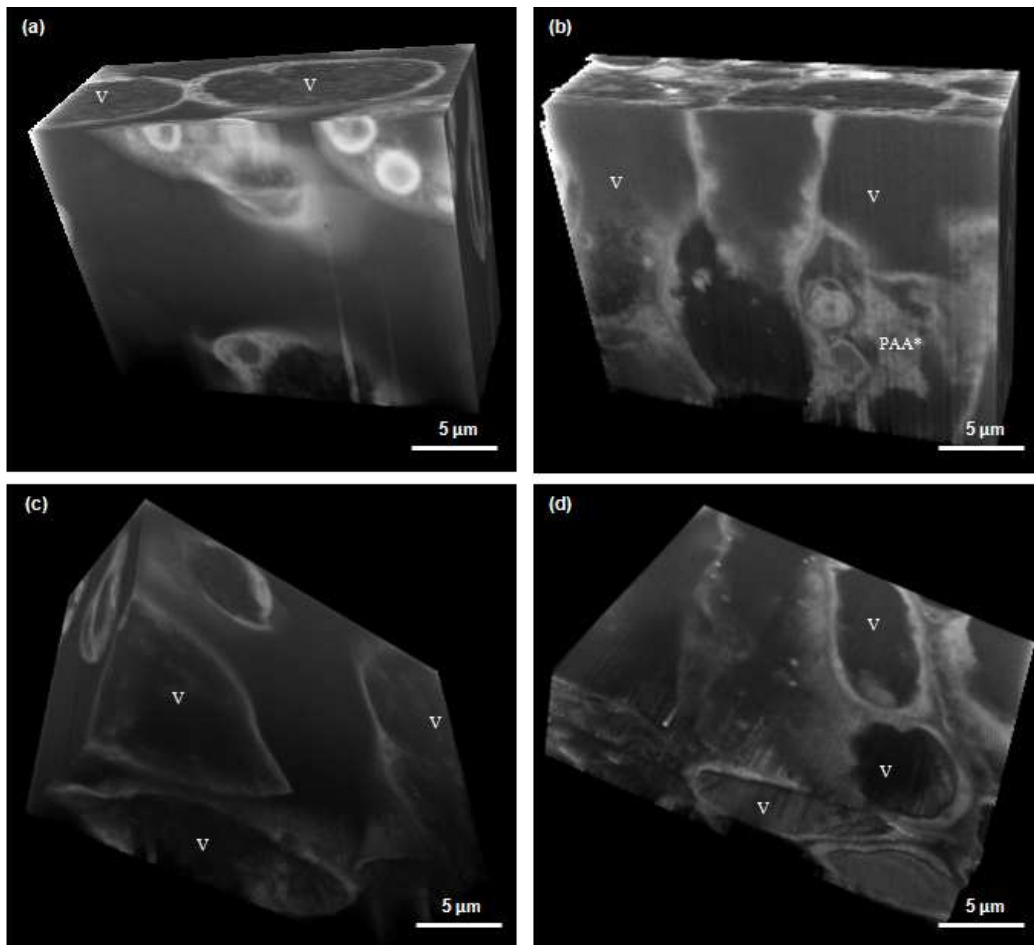


Figure 3.8: Orthographic projection of 3D reconstructed blocks of petal tissue from *B. juncea* and *C. bulbosa* using FIB-SEM.

(a – b) Front face of the tissue block from *B. juncea* showing abaxial epidermal cells with a few organelles, and large vacuoles with dispersed vacuolar content and *C. bulbosa* showing adaxial epidermal cells with a few organelles and PAA-like structures,

(c - d) Back face of the tissue block from *B. juncea* showing mesophyll cells with big vacuoles containing speckles of cytoplasmic content and *C. bulbosa*, showing mesophyll minimal cytoplasmic content and some vacuolar trafficking.

Serial sectioning and reconstruction videos of *A. thaliana*, *B. juncea* and *C. bulbosa* are available at:

Video 2a:

https://www.youtube.com/watch?v=d84IwnMVy-g&list=UU1u_lj0_RaWmJEwens0yBaQ

Video2b:

https://www.youtube.com/watch?v=nrgpfgGGRQ&list=UU1u_lj0_RaWmJEwens0yBaQ

Q

This developmental gradient is maintained in the fully expanded petal where the base is light green but the fully expanded portion of the petal is white. The observed PAAs from different sections of fully mature petals were most prominently observed in the petal lamina that mostly lack intact chloroplasts or the petal cells which have completed the chloroplast to leucoplast transition. Cells in the green base lacked PAAs.

Arabidopsis petals are white, which rules out the possibility that the observed PAAs contain carotenoid or anthocyanin pigmentation. It has been shown in other studies that during leaf senescence thylakoid pigment protein is degraded and stored in vacuoles (Martinoia et al., 2000) and during petal senescence cytoplasmic components are observed in the vacuole and relocalization of nutrients takes place (Thomas et al., 2003; Avila-Ospina et al., 2014; Matile and Winkenbach, 1971). The coincidence of PAA accumulation with the green to white transition suggest they result from chloroplast degradation and the accumulation of the broken down membrane and pigments into vacuoles (relocalization of nutrients), which could be used later if needed.

In comparison to *A. thaliana*, *B. juncea* TEM micrographs and 3D reconstruction from FIB-SEM revealed random disorganized electron dense particles in the vacuole that never aggregate to form a PAA. But remain randomly distributed throughout the life of the cell (Figures 3.7 and 3.8). *C. bulbosa* petals showed some resemblance with *A. thaliana* in terms of having high vacuolar trafficking and structures resembling PAAs but they were not as well defined as those seen in *A. thaliana* petals. Micrographs and 3D reconstruction from all three species revealed that well defined PAA's were seen in *A. thaliana* petals, less defined PAAs were also visible in another white-flowered species of

the same family, and no PAAs were seen in a yellow flowered species of the same family. This indicated a phenomenon or mechanism that occurs in petals which leads to PAA formation while the petal undergoes chloroplast to leucoplast transition.

The exploration of PAA development in *A. thaliana* allowed the recognition of six defined stages; 1 – densely cytoplasmic cell in the base of the petal with well defined chloroplasts, 2 – an early transitional stage where the cytoplasm ring is diminishing and electron dense particles are beginning to form in the vacuole, 3 – a late transitional stage where the electron dense particles are aggregating, 4 – a fully formed PAA in a cell with a thin ring of cytoplasm, 5 – transition stage where organelles are beginning to lose their integrity, and 6 – a dead petal cell. These stages are represented in a diagrammatic format in Figure 3.9 and as seen in electron micrographs in Figure 3.10a-f.

CONCLUSION

We hypothesized that the formation of PAAs is a result of the transition of chloroplasts to leucoplasts and that these structures are made of membrane and pigment remnants. TEM and FIB-SEM micrograph data of *A. thaliana* petals revealed that green cells at the base do not have PAAs but that fully developed white cells do have PAAs. The PAAs are maintained in these cells until apoptosis is complete and the tonoplast has ruptured. In addition, PAAs are absent in yellow *B. juncea* petals containing chromoplasts instead of leucoplasts. These data show that the formation of PAA's in the central vacuole is not only an indication of cell maturation and senescence but closely coincides with the transition of chloroplasts to leucoplasts in white petals of two species of the Brassicaceae. This fails to reject the initial hypothesis but can only suggest the content of the PAA.

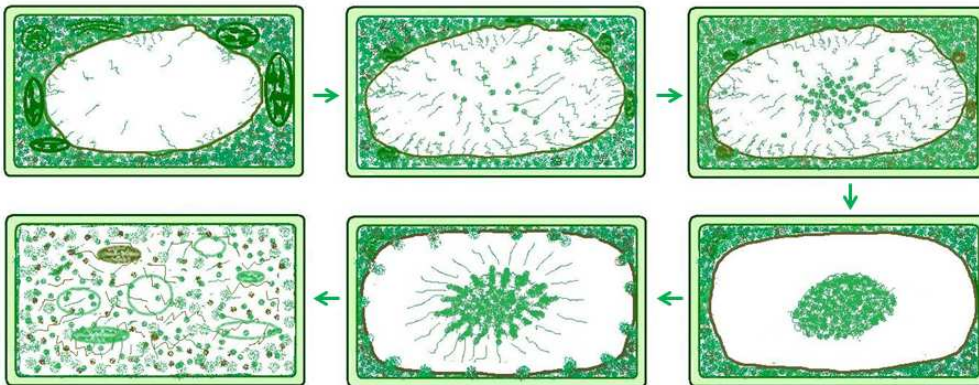


Figure 3.9: Diagrammatic representation of six stages of a petal cell's life and PAA formation observed in *A. thaliana* petal.

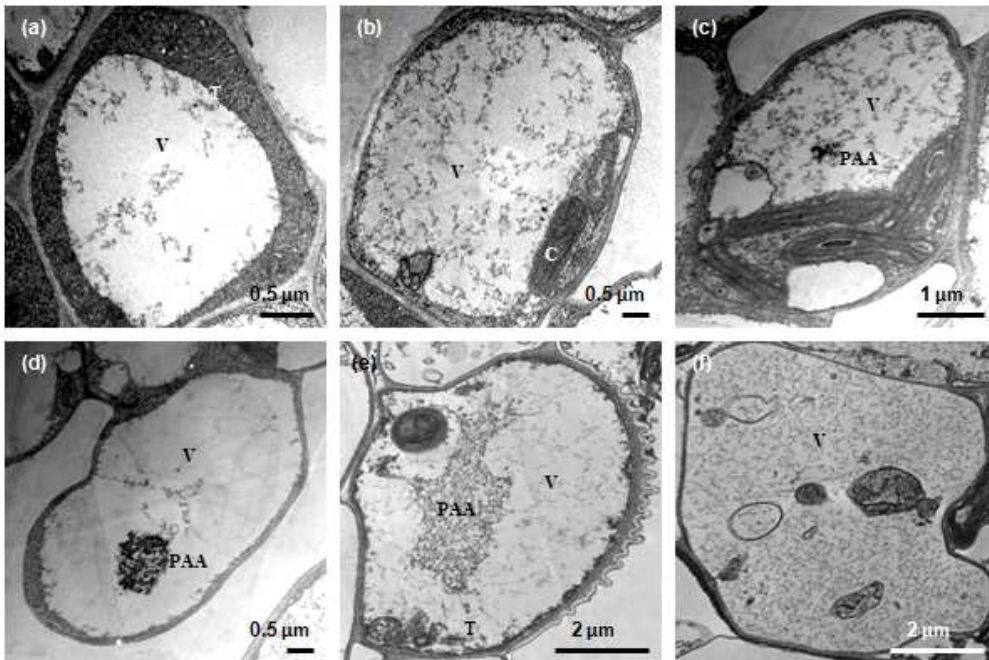


Figure 3.10: TEM micrographs of six stages of PAA development

a) Cell from the green base of an *Arabidopsis* petal showing thick cytoplasm with a big central vacuole and beginning of trafficking of cytoplasmic content to the vacuole via tonoplast, b) Cell showing reduced cytoplasm and increased trafficking, c) Cell showing beginning of formation of amorphous aggregate, and plastid transition from chloroplasts to leucoplasts, d) Cell with highly reduced cytoplasm and prominent amorphous aggregate, e) Cell showing tonoplast and amorphous aggregate degradation, f) cell showing complete degradation of tonoplast and amorphous aggregate.

REFERENCES

- Avila-Ospina L, Moison M, Yaoshimoto K, Masclaux-Daubresse. Autophagy, plant senescence, and nutrient recycling. *Journal of Experimental Botany*. 2014;65:3799-3811.
- Bhawana, Miller JL, Cahoon AB. 3D Plant Cell Architecture of *Arabidopsis thaliana* (Brassicaceae) Using Focused Ion Beam–Scanning Electron Microscopy. *Applications in Plant Sciences*. 2014;2:1-9.
- Droon WGV. Effects of pollination on floral attraction and longevity. *Journal of Experimental Botany*. 1997;48:1615-1622
- Echeverria E. Vesicle-mediated solute transport between the vacuole and the plasma membrane. *Plant Physiology*. 2000;123:217-1226.
- Egea I, Barsan C, Bian W et al. Chromoplast differentiation: current status and perspectives. *Plant Cell Physiology*. 2010;51:1601-1611.
- Hortensteiner S, Feller U. Nitrogen metabolism and remobilization during senescence. *Journal of Experimental Botany*. 2002;53:927-937.
- Irish VF. The *Arabidopsis* petal: a model for plant organogenesis. *Trends in Plant Science*. 2008;13:1360-1385.
- Irish VF. The flowering of *Arabidopsis* flower development. *The Plant Journal*. 2010;61:1014-1028.
- Jones ML. Mineral nutrient remobilization during corolla senescence in ethylene-sensitive and insensitive flowers. *AoB PLANTS*. 2013;5:ptl 023
- Kenichi S, Tomoko N, Kazuo I. Pollination induces autophagy in petunia petals via ethylene. *Journal of Experimental Botany*. 2013;64:1111-1120.
- Mara CD, Huang T, Irish VF. The *Arabidopsis* floral homeotic proteins APETALA3 and PISTILLATA negatively regulated the BANQUO genes implicated in light signaling. *The Plant Cell*. 2010;22:690-702.
- Martinoia E, Massonneau A, Frangne N. Transport process of solutes across the vacuolar membrane of higher plants. *Plant Cell Physiology*. 2000;41:1175-1186.
- Matile P, Winkenbach F. Function of lysosomes and lysosomal enzymes in the senescing corolla of the morning glory (*Ipomoea purpurea*). *Journal of Experimental Botany*. 1971;73:759-771.

Matile P, Hortensteiner S. Chlorophyll degradation. *Annual Review of Plant Physiology and Plant Molecular Biology*. 1999;50:67-95.

Mikula A, Tykarska T, Zielinska M, Kuras M, Rybczynski JJ. Ultrastructural changes in zygotic embryos of *Gentiana punctata* L. during callus formation and somatic embryogenesis. *Acta Biologica Cracoviensia. Series Botanica*. 2004;46:109-120.

Pyke KA, Page AM. Plastid Ontogeny during petal development in *Arabidopsis*. *Plant Physiology*. 1998;116:797-803.

Shumway LK, Cheng V, Ryan CA. Vacuolar protein in apical and flower-petal cells. *Planta*. 1972;106:279-290.

Smyth DR, Bowman JL, Meyerowitz EM. Early flower development in *Arabidopsis*. *The Plant Cell*. 1990;2:755-767.

Swanson SJ, Bethke PC, Zones RL. Barley aleurone cells contain two types of cuoles: characteristics of lytic organelles by use of fluorescent probes. *The Plant Cell*. 1998;10:685-698.

Thomas H, Ougham HJ, Wagstaff C, Stead AD. Defining senescence and death. *Journal of Experimental Botany*. 2003;54:1127-1132.

Weston EL, Pyke KA. Development Ultrastructure of cells and plastids in petals of Wallflower (*Erysimum cheiri*). *Annals of Botany*. 1999;84:763-769.

Whatley JM. The ultrastructure of plastids in the petals of *Caltha palustris* L. *New Phytologist*. 1984;97:227-231.

CHAPTER FOUR

SURFACE DECONTAMINATION OF PLANT TISSUE EXPLANTS

WITH CHLORINE DIOXIDE GAS

Bhawana, Jeannie M. Stubblefield, Anthony L. Newsome

&

A. Bruce Cahoon

Submitted To: In Vitro Cellular and Developmental Biology-Plant.

April, 2014.

(Provisionally Accepted)

ABSTRACT

The surfaces of plant tissues readily harbor bacteria, fungi, and spores making their preparation and growth by aseptic micropropagation difficult. Recent innovations in chlorine dioxide (ClO₂) gas production now allow for the production of small amounts of the gas to meet specific needs. This report demonstrates the efficacy of ClO₂ gas in the preparation of plant tissues for micropropagation. Cauliflower curd was surface decontaminated with 1500, 600, 300, and 150 ppm of gas for 30, 60, 180, and 360 minutes and the presence of surface microbioata was assayed. The use of ClO₂ gas in this system decontaminated cauliflower curd surfaces at rates equal to bleach treatment but the ClO₂ treated tissues grew more quickly and were healthier than the bleach treated samples. ClO₂ gas potentially represents an easy means to surface decontaminate plant tissues intended for micropropagation that when properly used does not pose a risk to human health.

INTRODUCTION

One of the challenging aspects of plant micropropagation is the eradication of viable microorganisms from the surfaces of explants intended for aseptic culture. Vegetative bacterial cells, dormant spores, and fungal hyphae adhere to the irregular plant tissue surface. This microbioata is difficult to remove or inactivate, and can quickly cause significant losses to commercial plant propagation operations or studies requiring plant tissue culture (Adams and Hartley 1898; Liao and Sapers, 2000). In addition, widely used disinfectants often do not kill or remove all dormant spores which may germinate in days or months after a seemingly aseptic culture has been initiated.

Numerous compounds such as ethanol, mercuric chloride, calcium hypochlorite, sodium hypochlorite, hydrogen peroxide, bromine water, silver nitrate, silver chloride, benzylkonium chloride, and antibiotics have been used to remove or inactivate biological contaminants associated with plant tissues (Sathyanarayana and Varghese 2007; Beyl 2000; Yeoman and Street 1977). All of these compounds are toxic to the plant tissues and balancing the eradication of viable contaminating microbioata versus explant viability can be difficult. In addition, some of these compounds present safety risks and produce hazardous waste that requires special handling procedures for use and disposal. Sodium hypochlorite (household bleach) is the most commonly used reagent due to its relative effectiveness versus low cost and accessibility.

Chlorine dioxide (ClO_2) gas and solutions have been used to meet a variety of disinfection needs for decades. Widespread use of the gas has been limited because it is too unstable for shipment and must be prepared at the application site. Historically, this

has required the use of dedicated equipment and trained personnel for ClO₂ gas generation. More recent advances in ClO₂ gas generation technology, however, have made possible the cost-efficient generation for smaller applications. Previous studies from this laboratory have demonstrated the antibacterial properties of ClO₂ gas generated by an easily used portable ClO₂ gas generation system (ICA Tri Nova, Newnan, Ga., USA) consisting of two granular precursors (sodium chlorite plus an activator). When placed together ClO₂ gas can be generated to meet a specific application need (Newsome et al., 2009; Salehzadeh, 2008; Newsome and Stubblefield, 2011).

The purpose of this investigation was to document the efficacy of an inexpensive and easily applied ClO₂ gas system to inactivate surface bacteria and fungi associated with plant surfaces for subsequent introduction into aseptic culture. For this, cauliflower (*Brassica oleracea*) curd explants were treated with ClO₂ gas and compared to the more traditional bleach treatment. Results suggested that ClO₂ gas could inactivate plant surface microorganisms at a rate comparable to bleach treatments but with greater tissue viability. This system offers an effective alternative gas based procedure to support plant micropropagation that does not produce hazardous solid waste and has negligible human health risks. Results also suggest ClO₂ gas treatments may have wide application for use in promoting the propagation of plants from cuttings in many different plant tissue culture settings.

MATERIALS AND METHODS

Plant Tissue

Cauliflower curd was chosen to test the efficacy of the antimicrobial ClO₂ gas generation system. The large surface area of the densely branched termini that make up cauliflower tissue, and its relatively quick response time in shoot culture make it an appropriate candidate for the gas studies. Cauliflower heads were purchased from a commercial market and the curd cut into small explants (10-15 mm²) using a sterile blade.

Inactivation of plant surface associated microbiota

For bleach treatment, tissues were washed for 20 minutes in 1% sodium hypochlorite with 0.1% Tween 20. Explants were washed three times with sterile water before introducing them to culture media.

Explants were treated with ClO₂ gas generated by the dry powder system produced by ICA Tri Nova (Newnan, Ga., USA, catalog #SF-GKF-002T). With this system, ClO₂ gas is generated when equal portions of proprietary powder 'A' (sodium chlorite) is mixed with activator powder 'B'. Explants were placed in a 1 liter glass dish with a plastic lid purchased at a kitchen supply store. Equal portions of each of the dry ClO₂ generation system components were mixed and placed in the glass dish taking care to prevent the powders from touching any of the tissue. Chlorine dioxide gas was generated according to the manufacturer's instructions to produce the following estimated peak concentrations - 1,500 ppm (1.3 g of each powder), 600 ppm (0.52g), 300 ppm (0.26 g), or 150 ppm (0.13 g). Explants and powders were left in the closed containers for 30, 60, 180, or 360

minutes. There were likely small variations in the concentration of gas during the treatment time due to yield escalation during the initial minutes of treatment followed by consumption due to oxidant demand from cauliflower explants. The amount of ClO₂ gas in the treatment containers was estimated based on previously established yield curves that were generated during treatment of organic materials such as fruits and plant cuttings which have a similar oxidant demand (personal communication, ICA Tri-Nova). After incubation the containers were opened in a laminar flow hood and explants were placed into culture medium.

Culture Media and Conditions

Plant surface decontamination was assessed by incubating treated explants in trypticase soy broth (TSB) for 14 days at 25°C. TSB (Becton, Dickinson and Company, Sparks MD, USA). TSB is a general purpose medium that supports the multiplication of a wide variety of bacteria. Explant viability was tested by placing treated tissues on shoot induction medium (MS-S) containing 1X Murashige and Skoog salts and vitamins (Murashige and Skoog 1962), 3% sucrose, 200 mg/L myoinositol, 0.5 mg/L BAP, 1 mg/L NAA, 1mg/L IAA, 1 mg/L 2,4-D, and 0.8% plant tissue culture agar, pH 5.7, for 21 days at 25°C.

Experimental Design

A TSB based assay was used to determine the presence of bacteria remaining on the surface of treated and untreated cauliflower explants. This assay was replicated twice with two different cauliflower heads purchased at different times. For each replicate ten

curd explants were exposed to each treatment – 150, 300, 600, and 1500 ppm ClO₂ at 30, 60, 180, and 360 minutes. Equal numbers of explants were also bleach treated, autoclaved (negative control), or left untreated (positive control). Treated tissues and controls were submerged in TSB medium and incubated at 25°C for 14 days to encourage growth of microorganisms. Cultures were scored as positive for bacteria if the culture became turbid during the 14 day incubation period.

Tissue viability and culture efficacy were assayed by placing ten curd explants treated with 600 or 300 ppm ClO₂ for 360 minutes, 1500 or 600 ppm ClO₂ for 180 minutes, 1500 ppm ClO₂ for 60 minutes, onto MS-S medium (described above). Bleach treated and untreated samples were also cultured as controls. This assay was performed with two replicates with two cauliflower curds purchased at different times.

Data collected from replicates were averaged, the standard error calculated, and graphed for each experiment.

RESULTS

Cauliflower curd explants were treated with a range of ClO₂ concentrations (150, 330, 600, and 1500 ppm) for four different lengths of time (30, 60, 180, and 360 minutes) to determine if the gas would inactivate plant surface microbiota without compromising explant viability for tissue culture. Microbiota viability was determined by submerging treated portions of curd into TSB to encourage growth of viable microorganisms.

Turbidity in the TSB medium was scored as recovery of viable microbiota. Absence of turbidity was scored as a lack of microbial viability and growth. For comparative

purposes, duplicate explant tissues were treated with bleach, autoclaved (positive control), or left untreated (negative control). A separate set of duplicate tissues were incubated on MS-S medium to determine explant viability. This was measured as the ability of the white curd to turn green and produce shoots. Tissues treated with 1500 ppm chlorine dioxide for 60 or 180 minutes, 600 ppm for 180 or 360 minutes, and 300 ppm for 360 minutes resulted in tissues that were rendered free of recoverable surface microbioata at a rate comparable to or greater than bleach treatments (Figure 4.1). Most of the ClO₂ treatments gave rise to viable explant tissue as measured in small scale (n=6, one replicate) MS-S assays (Figure 4.1).

Tissues treated with 1500 ppm for 360 minutes had no detectable growth of microbioata but also did not respond in MS-S medium suggesting the upper limit of tissue viability to ClO₂ gas had been exceeded. The ClO₂ treatments which produced the most promising results were identified and subsequent replicates performed. Further replicates yielded results analogous to the initial TSB and MS-S assays (Figure 4.2).

ClO₂-treated tissues had a brown oxidized appearance (Figure 4.3A). A qualitative assessment of tissue viability suggested that the browning may have only affected the outermost layers of cells since the explants were still able to initiate shoot production (Figures 4.3C-G). . Visual inspection of tissues treated with ClO₂ gas also suggested this strategy had a less detrimental effect on the tissue than the more conventionally used bleach treatment to eliminate plant surface microbiota (Figure 4.4).

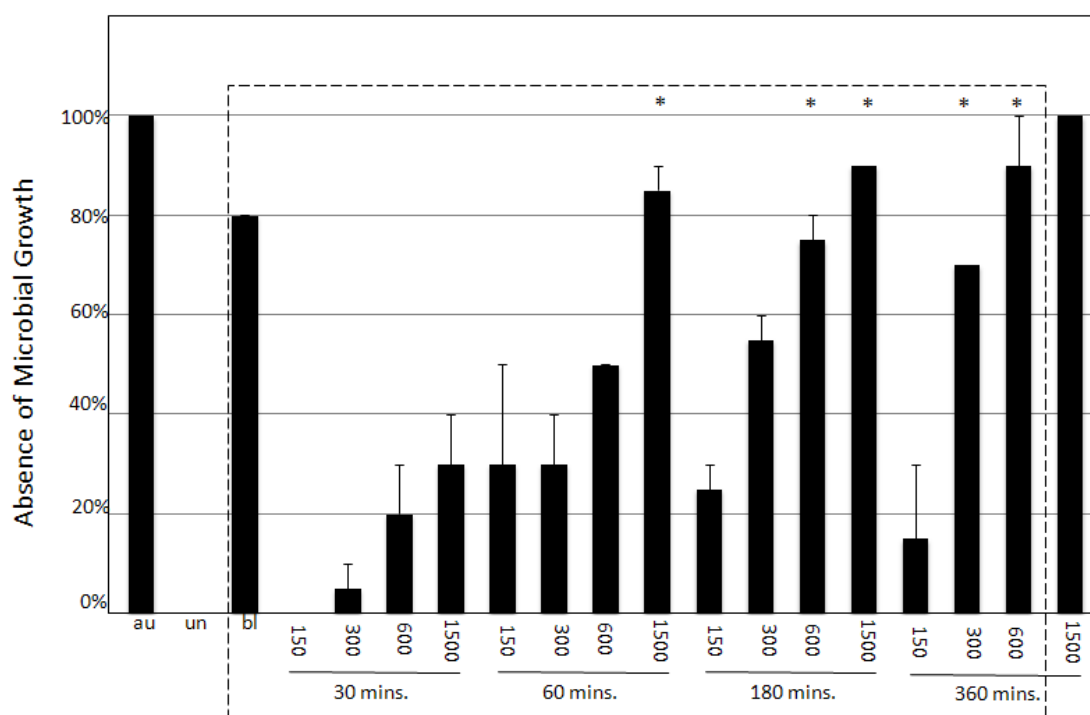


Figure 4.1: Results of TSB assay showing inactivation of cauliflower curd surface microbioata using ClO₂ gas generated with Fast Release powder. Lane au – autoclaved tissues; un – untreated; bl – surface decontaminated using bleach; 150, 300, 600, or 1500 – estimated peak ppm ClO₂; 30, 60, 180, or 360 minutes – time of treatment. The y-axis represents the average number ± standard error of TSB cultures that remained clear suggesting no bacterial growth. Tissues treated under conditions within the dashed line box were viable and produced shoots on MS-S medium. Asterisks denote the most promising conditions chosen for further testing.

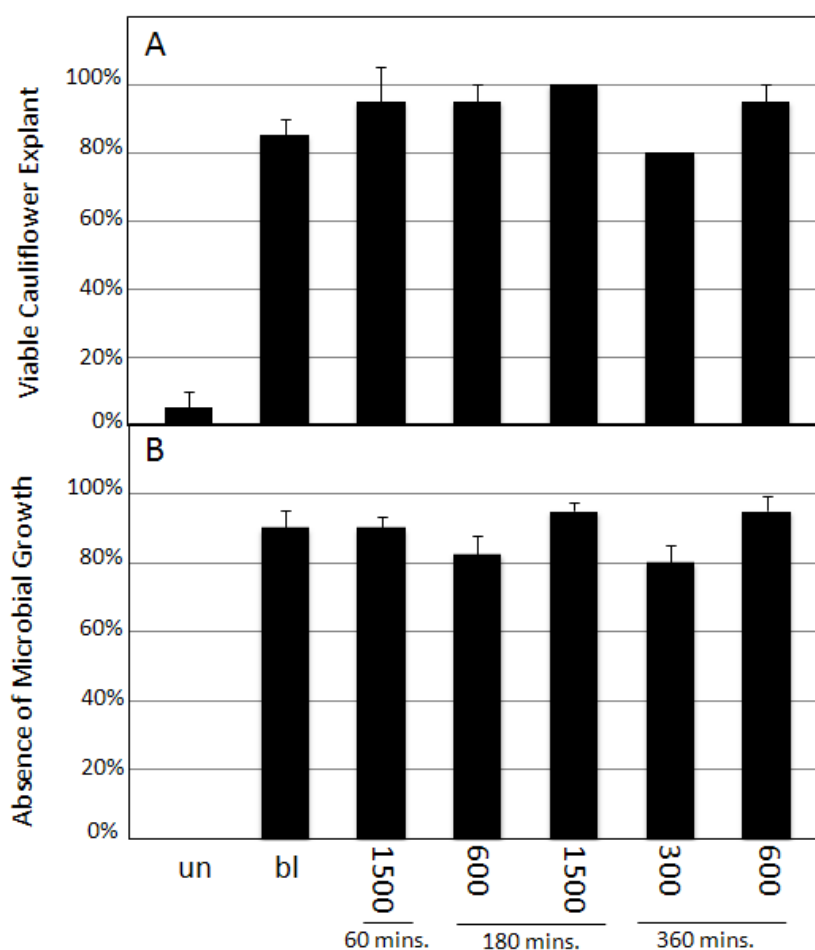


Figure 4.2: Impact of the most promising ClO_2 gas treatments on elimination of viable microbioata and subsequent cauliflower curd explant viability. un – untreated; bl – surface decontaminated using bleach; 150, 300, 600, or 1500 – estimated peak ppm ClO_2 ; 30, 60, 180, or 360 minutes – time of treatment. (A) The average number \pm standard error of viable cauliflower explants from two replicates is shown. All non-contaminated cultures were productive and were counted as viable. (B) The average number \pm standard error of non-turbid cultures from four replicates with standard error bars is shown.

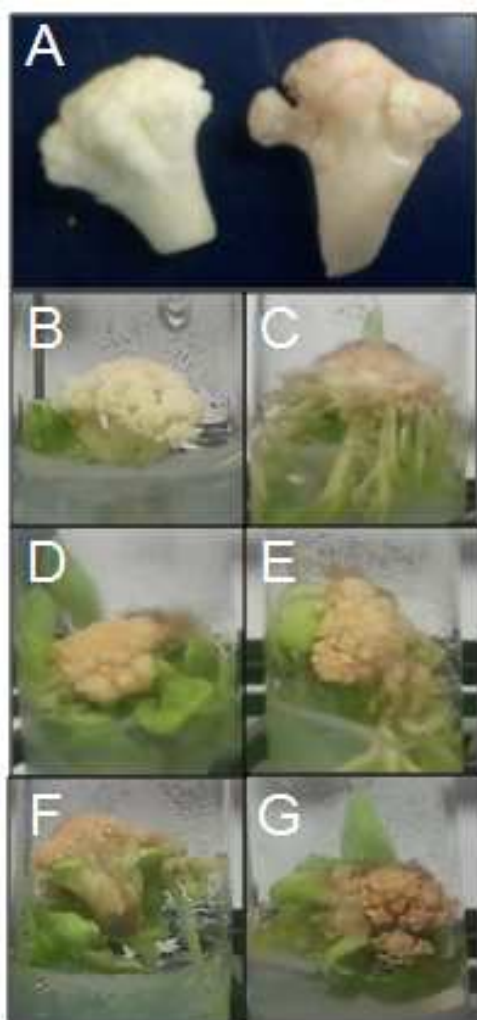


Figure 4.3: Tissue discoloration and viability after chlorine dioxide treatments.

A – An untreated explant (left) and chlorine dioxide treated (right) immediately after exposure. Explants cultured in MS-S medium two weeks after treatment with bleach (B), 300 estimated peak ppm ClO_2 for 360 mins. (C), 600 ppm 180 mins. (D), 600 ppm 360 mins. (E), 1500 ppm 60 mins. (F) and 1500 ppm 180 mins. (G).

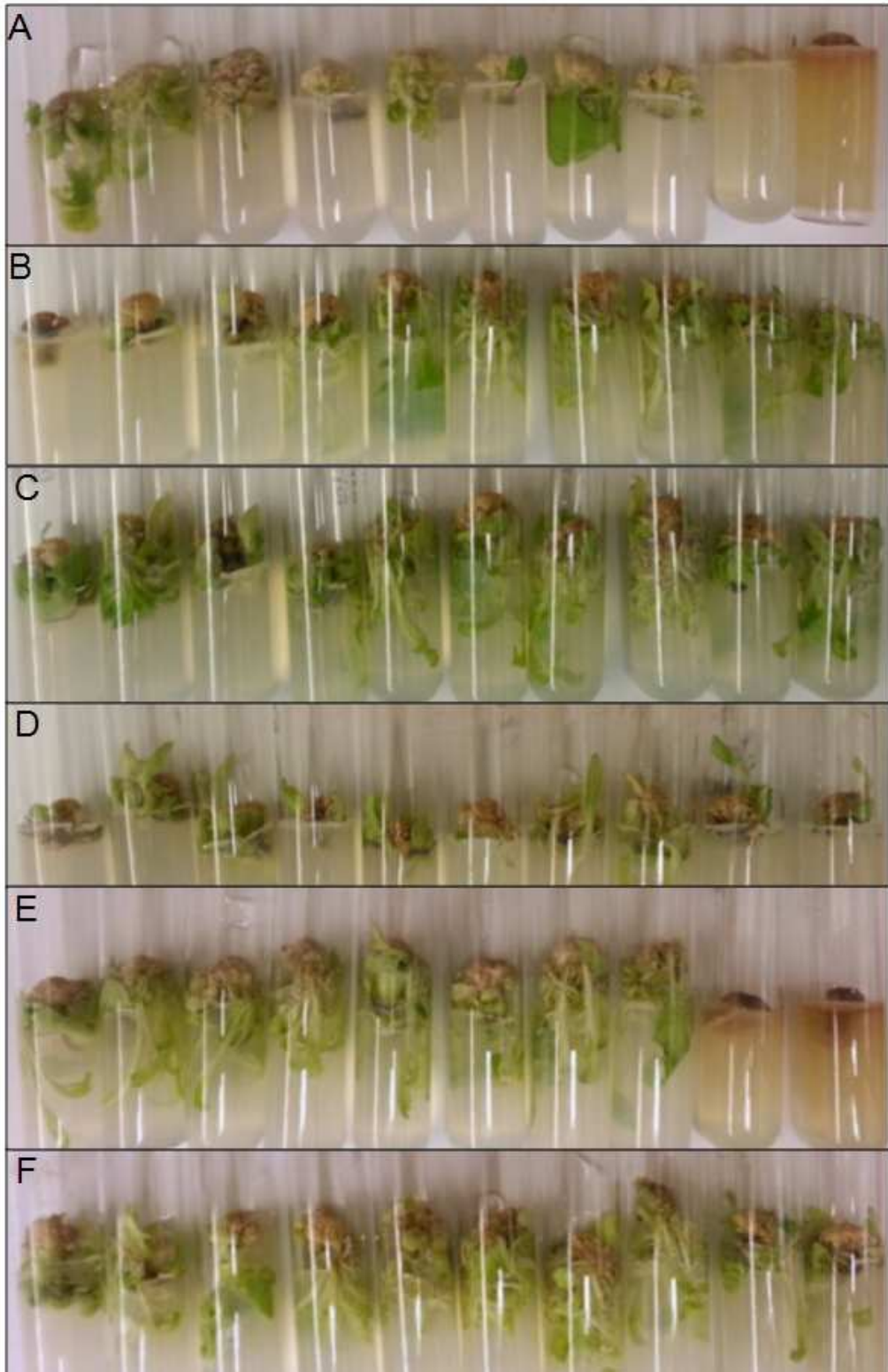


Figure 4.4: Shoot culture viability of cauliflower curd treated with ClO₂ gas. Ten portions of cauliflower curd were cleaned with bleach. (A), 60 minutes in 1500 estimated peak ppm ClO₂ gas (B), 180 minutes in 600 ppm (C), 180 minutes in 1500 ppm (D), 360 minutes in 300 ppm (E), or 360 minutes in 600 ppm (F). Treated tissues were placed on MS-S medium and incubated for 21 days at 25°C. Shoot tissues produced in this culture system often grow in a negatively geotropic manner regardless of the surface decontamination method.

DISCUSSION

Chlorine dioxide is a strong oxidizing agent and it has approximately 2.5 times the oxidation ability of chlorine (Benarde et al., 1965). It is also reported to be effective in disruption of biofilms and bacteria (Gagnon et al., 2005; Simpson et al., 1993). Because of its broad biocidal properties, in 1967 ClO₂ in solution was registered as a disinfectant and sanitizer by the United States Environmental Protection Agency (United States Environmental Protection Agency). Chlorine dioxide has been widely used for potable water preparation, wastewater treatment and food sanitation (Aieta and Berg, 1986; Gomez-Lopez et al., 2009; Simpson et al., 1993). The use of ClO₂ gas and solutions for use in intimate human activities or products that may be consumed by humans is additionally supported by the reported absence of cumulative adverse health effects when properly used (United States Department of Health and Human Services). Chlorine dioxide is also not considered carcinogenic or to be a reproductive hazard (United States Department of Health and Human Services). More recent studies have suggested that ClO₂ gas can be more effective than ClO₂ disinfecting solutions in eliminating bacteria on irregular surfaces such as animal skin and it was proposed the gas was more effective in penetrating the irregular skin surface that could harbor bacteria (Newsome and Stubblefield, 2011).

The excellent biocidal properties of ClO₂ gas along with its favorable toxicity properties have suggested its use against human pathogens that could reside on plant produce. Here its use has been viewed and used in terms of promotion of human health by inactivating pathogens that may be associated with plants consumed by humans. This activity is

supported also by demonstrating ClO₂ gas treatment of plant produce results in minimal to no detectable chemical residues and poses an insignificant risk for subsequent human consumption (Trinetta et al., 2011). A major concern in human consumption of plants or plant products is *Escherichia coli* O157:H7. On apple surfaces ClO₂ gas was effective in the elimination of this pathogen (Du et al., 2003). Comparative studies have suggested that gaseous ClO₂ treatments are more effective in the elimination of surface bacteria on plant tissue than washing or use of disinfection solutions (Singh et al., 2002). The bacterial burden of *E. coli* O157:H7 on basil and lettuce leaves could also be significantly reduced with ClO₂ gas (Ortega et al., 2008). The gas also demonstrated good efficacy on plant produce against other human pathogens such as *Salmonella* and *Listeria*. Here it was demonstrated these gas treatments were also effective against yeasts and molds associated with plant produce (Sy et al., 2005a; Sy et al., 2005b; Wu and Kim, 2007).

A logical extension of these studies is a determination of the suitability of ClO₂ gas treatments to reduce or eradicate microbes that can diminish outgrowth in aseptic culture of plant explants. Here the desired outcome is not the reduction or elimination of specific human microbial pathogens, but rather the elimination of bacteria, yeast, and molds that can cause loss in subsequent plant propagation from the explants. For this determination ClO₂ gas treatments were compared to the often used sodium hypochlorite (bleach) treatment. Using a cauliflower curd model system, ClO₂ gas could be used to eliminate viable microbioata at a level equivalent to sodium hypochlorite. The elimination of microbioata by ClO₂ gas was achieved without severely compromising viability for micropropagation. The favorable results observed in the current study are likely at least in

part a reflection of two ClO₂ gas properties. First, results could be attributed to its strong oxidizing properties. Secondly, it is likely that the gas phase of ClO₂ is more proficient than liquid disinfectants in penetrating porous niches on plant tissues that can harbor microbioata that are detrimental to the outgrowth of plant explants.

Micropropagation of plants has been in place since the late 1950s and early 1960s. It allows for the creation of large numbers of plants from small fragments (explants) of a stock plant. Clean stock material and explants free of plant microbial pathogens are key factors in the creation of healthy plants. Since the inception of micropropagation, the reduction or elimination of the plant microbial pathogens has been an enduring problem which still frequently causes significant plant loss. Unfortunately, there have not been recent developments for improving the sanitation of plant explants for micropropagation. Sodium hypochlorite has been widely used and served as a mainstay in the disinfection of plant explants for subsequent propagation. It is readily available and inexpensive. However, bleach can be highly damaging to plant tissue thus diminishing explant viability. In addition, its ability to eliminate plant associated microbioata is often not ideal. When compared to bleach, certain concentrations of ClO₂ gas were more effective in eliminating damaging microbioata and in promoting the outgrowth of healthy plant explants.

The development of inexpensive, highly portable, and easily used ClO₂ gas generating technologies have made this gas available for more widespread use and novel applications as outlined in this study. This technology likely would be of interest and has the potential to serve individuals with a personal interest (hobbyists) in the outgrowth of

plant explants and those engaged in a larger setting with commercial interests in the outgrowth of plant explants.

CONCLUSION

Results of the current study suggest a novel application for the use of ClO₂ gas that has potential benefit to individuals and industrial groups engaged in micropropagation of plant explants.

ACKNOWLEDGEMENT

The authors wish to thank MTSU's Department of Biology and the Molecular Biosciences Program for supporting this work. The chlorine dioxide dry powder generation system was provided by ICA TriNova, Newnan, Ga., USA.

REFERENCES

- Adams MR, Hartley AD. Factors affecting the efficacy of washing procedures used in the production of prepared salads. *Food Microbiology*. 1989;6:69-77.
- Aieta EM, Berg JD. A review of chlorine dioxide in drinking water treatment. *Journal of American Water Works Association*. 1986;78:62-70.
- Benarde MA, Israel MM, Oliveri VP, Granstrom ML. Efficacy of chlorine dioxide as a bactericide. *Applied and Environmental Microbiology*. 1965;13:776-780.
- Beyl CA. Getting started with tissue culture – media, preparation, sterile technique, and laboratory equipment. In: Trigliano RN and Gray DJ (eds) *Plant Tissue Culture Concepts and Laboratory Exercises*. 2nd edn. CRC Press; 2002.
- Du J, Han Y, Linton RH. Efficacy of chlorine dioxide gas in reducing Escherichia coli O157:H7 on apple surfaces. *Food Microbiology*. 2003;20:583-591.
- Gagnon GA, Rand JL, O’Leary KC, Rygel AC. Disinfectant efficacy of chlorite and chlorine dioxide in drinking water biofilms. *Water Research*. 2005;39:1809-1817.
- Gomez-Lopez VM, Rajkovic A, Ragaert P, Smigic N, Devlieghere F. Chlorine dioxide for minimally processes produce preservation: a review. *Trends in Food Science & Technology*. 2009;20:17-26.
- Liao CH, Sapers GM. Attachment and growth of Salmonella Chester on apple fruits and in vivo response of attached bacteria to sanitizer treatments. *Journal of Food Protection*. 2000;63:876-883.
- Murashige T, Skoog F. A revised medium for rapid growth and bioassays with tobacco tissue cultures. *Physiologia Plantarum*. 1962;15:473-497
- Newsome AL, DuBois JD, Tenney JD. Disinfection of football protective equipment using chlorine dioxide produced by the ICA TriNova system. *BMC Public Health* . 2009;9:326-334.
- Newsome AL, Stubblefield JM. Novel disinfection applications using a portable chlorine dioxide gas generation system. Report on the 2011 U.S. Environmental Protection Agency (EPA) Decontamination Research and Development Conference. 2011;61-62.
- Ortega YR, Mann A, Torres MP, Cama V. Efficacy of gaseous chlorine dioxide as a sanitizer against *Cryptosporidium parvum*, *Cyclospora cayetanensis*, and *Encephalitozoon intestinalis* on produce. *Journal of Food Protection*. 2008;71:2410-2414.
- Salehzadeh I. Decontamination assessment of *Bacillus atrophaeus* spores on common surfaces using chlorine dioxide gas and a novel device. MS thesis, Middle Tennessee State University, USA

Simpson GD, Miller RF, Laxton GD, Clements WR. A focus on chlorine dioxide: the ideal biocide. Paper No 472, Corrosion 93, New Orleans, La. March 8-12, 1993.

Singh N, Singh RK, Bhunia AK, Stroshine RL. Efficacy of chlorine dioxide, ozone, and thyme essential oil or a sequential washing in killing *Escherichia coli* 0157:H7 on lettuce and baby carrots. *LWT-Food Science and Technology*. 2002;35:720-729.

Sathyanarayana BN, Mathews D. Plant Tissue Culture: Practices and New Experimental Protocols. I K International Publishing House; 2007.

Sy KV, McWatters KH, Beuchat LR. Efficacy of gaseous chlorine dioxide as a sanitizer for killing *Salmonella*, yeasts, and molds on blueberries, strawberries, and raspberries. *Journal of Food Protection*. 2005;68:1165-1175.

Sy KV, Murray MB, Harrison MD, Beuchat LR. Evaluation of gaseous chlorine dioxide as a sanitizer for killing *Salmonella*, *Escherichia coli* 0157:H7, *Listeria monocytogenes*, and yeasts and molds on fresh and fresh produce. *Journal of Food Protection*. 2005;68:1176-1187.

Trinetta V, Vaidya N, Linton R, Morgan M. Evaluation of chlorine dioxide gas residues on selected food produce. *Journal of Food Science*. 2011;76:T11-T15.

Online document: United States Department of Health and Human Services (US DHHS) (2004) Toxicological profile for chlorine dioxide and chlorite. Available at: <http://www.atsdr.cdc.gov/ToxProfiles/tp160.pdf> Accessed June 15, 2013.

Online document: United States Environmental Protection Agency (EPA) (2007) Anthrax spore decontamination using chlorine dioxide. Available at: <http://www.epa.gov/pesticides/factsheets/chemicals/chlorinedioxidefactsheet.htm>. Accessed June 8, 2013.

Wu V, Kim B. Effect of a simple chlorine dioxide method for controlling five foodborne pathogens, yeasts and molds on blueberries. *Food Microbiology*. 2007;24:794-800.

Yeoman MM, Street H E. Tissue (callus) cultures – techniques. In: Street HE (ed) Plant Tissue and Cell Culture. 2nd edn. University of California Press; 1977.

CONCLUSION

In this dissertation I describe the use of Focused Ion Beam-Scanning Electron Microscopy (FIB-SEM) to study plant sub-cellular anatomy and explore one overlooked sub-cellular anatomical feature, the petal amorphous aggregate.

A new methodology was developed as part of this work to adapt FIB-SEM for use on plant tissues. Chapter 2 of this dissertation explains the necessary modifications in the protocol and the benefits of using FIB SEM for plant tissue by successfully processing and reconstructing five different tissues from *Arabidopsis thaliana* in three dimensions. There are very few anatomical studies that take such a broad view and provide images of multiple tissues from a single species. The addition of the third dimension also provided intricate information about these tissues by revealing minute details about overall cell structure in each tissue, the type and number of organelles present in each cell, and their localization.

The three dimensional reconstruction of the plant tissue created an opportunity to explore some phenomenon which have previously been ignored either as artifacts or were considered irrelevant due to lack knowledge about the actual occurrence inside the cells. The second study (Chapter 3) describes one such structure I call the ‘Petal Amorphous Aggregate’ inside the petal cells of *A. thaliana*. A comparison of TEM micrographs and 3D reconstructions of petal cells and their vacuolar contents from three members of Brassicaceae family was used to test the hypothesis – PAAs form from the waste products produced during the transition from membrane dense chloroplasts to colorless leucoplasts. This study revealed the formation and disintegration of PAA’s as the petals

of *A. thaliana* turn white from green undergoing the chloroplast to leucoplast transition. A similar transition was observed in another white flowered member of the Brassicaceae family, *C. bulbosa* but PAAs were missing in the yellow flowered *B. juncea*. This suggested that the PAA formation coincides with the plastid transition and the PAA's are possible remnants of broken down chlorophyll and thylakoid membrane from chloroplast turning into leucoplast.

REFERENCES FOR INTRODUCTION AND CONCLUSION

- Archibald J. The puzzle of plastid evolution. *Current Biology*. 2009;19:81-88.
- Bhawana, Miller JL, Cahoon AB. 3D Plant Cell Architecture of *Arabidopsis thaliana* (Brassicaceae) Using Focused Ion Beam–Scanning Electron Microscopy. *Applications in Plant Sciences*. 2014;2(6):1300090.
- Bushby AJ, P'ng KMY, Young RD, Pinali C, Knupp C, Quantock AJ. Imaging three-dimensional tissue architectures by focused ion beam scanning electron microscopy. *Nature Protocols*. 2011;6:845–858.
- Carde JP. Leucoplasts: a distinct kind of organelles lacking typical 70S ribosomes and free thylakoids. *European Journal of Cell Biology*. 1984;34:18-26.
- Fowke LC. Transmission and Scanning Electron Microscopy for Plant Protoplasts, Cultured Cells and Tissues. *Plant Cell, Tissue and Organ Culture. Springer Lab Manual*. Springer Berlin Heidelberg; 1995:229-238.
- Giannuzzi LA, Kempshall BW, Schwarz SM, Lomness JK, Prenitzer BI, Stevie FA. FIB lift-out specimen preparation techniques. In Introduction to focused ion beams, L.A. Giannuzzi, and F.A. Stevie, eds. Springer, New York, New York, USA; 2005:201–228.
- Giannuzzi LA. Introduction to focused ion beams: Instrumentation, theory, techniques and practice. Springer, New York, New York, USA; 2005.
- Hoffmeister M, Martin W. Interspecific evolution: microbial symbiosis, endosymbiosis and gene transfer. *Environmental Microbiology*. 2003;5:641-649.
- Lopez E, Pyke K. Plastid unleashes: their development and their integration in plant development. *International Journal of Developmental Biology*. 2005;49:557-577.
- Merchan-Perez A, Rodriguez JR, Alonso-Nanclares L, Schertel A, DeFelipe J. Counting synapses using FIB/SEM microscopy: A true revolution for ultrastructural volume reconstruction. *Frontiers in Neuroanatomy*. 2009;3:18.
- Midgley PA, Wetland M. 3D electron microscopy in the physical sciences: the development of Z-contrast and EFTEM tomography. *Ultramicroscopy*. 2003;96:413-431.
- Miyagishima S, Takahara M. Plastid division is driven by a complex mechanism that involves differential transition of the bacterial and eukaryotic rings. *The Plant Cell*. 2001;13:2257-2268.
- Pyke k. Plastid biogenesis and differentiation. In R Bock, ed, Cell and Molecular Biology of Plastids, Vol. 19. Springer, Verlag Berlin Heidelberg: 1-28; 2007.
- Pyke K. Plastid Biology. Cambridge University Press: 1-38; 2009.

Sager R, Ishida MR. Chloroplast DNA in *Chlamydomonas*. *Proceedings of the National Academy of Sciences USA*; 1963:725-730.

Stokes DJ, Morrissey F, Lich BH. A new approach to studying biological and soft materials using focused ion beam scanning electron microscopy (FIB SEM). *Journal of Physics: Conference series*. 2006;26:50-53.

Sugiyama M, Sigesato G. A review of focused ion beam technology and its applications in transmission electron microscopy. *Journal of Electron Microscopy*. 2004;53:527–536.

Villinger C, Gregorius H, Kranz C et al. FIB/SEM tomography with TEM-like resolution for 3D imaging of high pressure frozen cells. *Histochemistry and Cell Biology*. 2012;138:549-556.

Wei D, Jacobs S, Modla S et al. High-resolution three-dimensional reconstruction of a whole yeast cell using focused-ion beam scanning electron microscopy. *BioTechniques*. 2012;53:41–48.

Wise RR. The diversity of plastid form and function. In: Wise RR and Hooper JK (eds) *The Structure and Function of Plastids. Advances in Photosynthesis and Respiration*. Springer, Dordrecht; 2006:3-26.

Xin C, Bhattacharya D. The origin of plastids. *Nature Education*. 2010;3:84.